Journal of Guidance, Control, and Dynamics,
Volume 45, Number 9, September 2022, pp. 1598-1613
DOI: 10.2514/1.G006850

Generalized Analysis of Biased Proportional Navigation Guidance with Fractional Power Error Feedback

Namhoon Cho *
Cranfield University, Cranfield, Bedfordshire, MK43 0AL, United Kingdom

Jinrae Kim †
Seoul National University, Seoul, 08826, Republic of Korea

Seokwon Lee ‡
Cranfield University, Cranfield, Bedfordshire, MK43 0AL, United Kingdom

Youdan Kim §
Seoul National University, Seoul, 08826, Republic of Korea

This study presents a comprehensive analysis of biased proportional navigation guidance laws with variable gain in the bias command that achieve stationary target interception with a desired impact angle under the restriction of permissible look angle. More specifically, this study investigates the bias shaping approach which takes the bias gain function given by a product of factors in range and look angle. The linear feedback and fractional power feedback of impact angle error are considered for command structures. For each command form, this study examines the conditions that should be satisfied by the gain functions to guarantee mission accomplishment without violation of the constraints. The analysis particularly focuses on estimating the set of feasible initial or final conditions that ensure compliance with the constraints along the trajectory. Numerical simulation is performed for a range of initial and final flight path angles to verify the analytical results. The findings of this study provides a general foundation for the design of a non-switching guidance law for impact angle control with limited look angle through shaping of gain profiles.

I. Introduction

Weight and cost reduction in modern tactical missiles poses a significant challenge in the design of guidance algorithms. Due to size constraints, seekers with limited field of view are typically employed for passive homing to meet design goals. The reduced field of view increases the complexity of hitting specifically a less protected spot on the

*Research Fellow, Centre for Autonomous and Cyber-Physical Systems, School of Aerospace, Transport and Manufacturing, nhcho91@gmail.com, AIAA Member

†Ph.D. Student, Department of Aerospace Engineering, kjl950403@gmail.com

‡Research Fellow, Centre for Autonomous and Cyber-Physical Systems, School of Aerospace, Transport and Manufacturing, seokwon.lee@cranfield.ac.uk, AIAA Member

§Professor, Department of Aerospace Engineering, Institute of Advanced Aerospace Technology, ydkim@snu.ac.kr, AIAA Associate Fellow

Published by AIAA. This is the Author Accepted Manuscript issued with: Creative Commons Attribution Non-Commercial License (CC:BY:NC 4.0).
The final published version (version of record) is available online at DOI:10.2514/1.G006850. Please refer to any applicable publisher terms of use.

target. One of the major difficulties is that maintaining visibility of the target reduces achievable impact angles and feasible launch angles relative to cases without look angle constraints. A physical consequence of this constraint on surface-to-surface engagement scenarios is that vehicles fly to higher altitudes as the desired impact angle becomes steeper. In this respect, the necessity to satisfy all given constraints while providing a wide coverage of the feasible region poses significant challenges to the design of a feedback guidance method.

Guidance laws that explicitly handle the impact angle condition as well as the look angle inequality constraint have been developed extensively for interception of a stationary target [1–20]. A structural commonality identified in a number of existing guidance laws is the multi-stage architecture which consists of steering policies for each phase and a logic for switching between different phases. A composite guidance scheme typically combines i) direct control [10] or indirect targeting [1, 6, 7, 9, 21] of impact angle on an unconstrained arc and ii) look angle boundary tracking on a constrained arc of a trajectory. The policy on a constrained arc is effectively deviated pure pursuit guidance law, which is equivalent to Proportional Navigation Guidance (PNG) with a navigation constant $N = 1$ [3, 10]. The methods in [2, 4, 7, 9] have a two-stage proportional navigation structure in which N switches over from one value to another once reaching a certain switching surface. The methods developed in [5, 10], based on linear quadratic regulator theory with the state inequality constraint, were conceived in a different multi-stage form. The method presented in [13] is also framed into many stages.

More advanced control design schemes have also been adopted to address the same problem, and the scope has been extended to handle moving targets. Nonlinear controllers proposed in [14–18, 20] utilize clever designs and avoid discontinuous command switching that may induce abrupt response. An online convex programming method based on the lossless convexification technique was proposed in [11] to incorporate all constraints in optimization, and its results are compared with the methods of [3] and [7]. The multi-stage algorithms have been extended to deal with the case of a non-maneuvering target in [21–24]. The methods presented in [21] and [22] are extensions of [2] and [3], respectively.

A Biased Proportional Navigation Guidance law (BPNG) with proper shaping of the bias command is shown to be a balanced solution that is practically useful and performant, however, a theoretical analysis supporting the design of bias gain functions has not been performed in a general setting. The method in [16] is a specific example of BPNG with a smooth bias gain function which is preferable for several reasons; i) smoothness of command, ii) robustness against uncertainties resulting from feedback, and iii) retention of intuitive features of widely-used PNG. Unlike most of the multi-stage methods, a BPNG substantially relies on the choice of the gain profile to attain wide coverage of the feasible trajectory space which is essential for the versatility to accomplish mission successfully in various situations. In this regard, it is necessary to establish certain design criteria.

Motivated by these observations, this study presents a generalized analysis of the BPNG considering a factorized form of gain function in the bias command. For our purpose, this study examines both the linear feedback and the fractional power feedback of the impact angle error. The primary objective is to rigorously clarify the necessary

conditions to guarantee satisfaction of the constraints imposed on miss distance, impact angle, and look angle. Another main objective is to discuss how the set of feasible geometric configurations depends on bias gain function, type of error feedback, and look angle limit. A particular concern in the analysis is given to the requirement of zero final bias command which is necessary for reliable homing performance in the presence of uncertainties.

The analytical results of this study complement earlier studies on BPNGs with generalized discussions relating desired response characteristics and bias gains. The analysis addresses convergence of impact angle error, convergence of look angle, boundedness of look angle, and feasible initial/final conditions. More specifically, this study presents a sufficient condition estimating the set of achievable impact angles or feasible launch angles, which is useful for mission planning despite the conservatism involved. This study also derives a sufficient condition for boundedness of look angle and zero final lateral acceleration without severely limiting the bias gain to a narrow class of functions.

This study extends our previous works on BPNG for control of impact angle under look angle constraint [15, 16, 25] in the following directions. First, the present study provides more complete analyses. New findings on the necessary and sufficient conditions for the impact angle error and the lateral acceleration to be zero at the final time are described in addition to the sufficient conditions discussed in [25]. Also, this study presents a novel approach to analyze convergence of look angle based on the Bernoulli differential equation. Most importantly, new guidelines for design of bias gains are proposed to aid practical designs. Second, the analytical results of this study are compared with those of relevant earlier studies. Third, this study compares linear feedback and fractional power feedback with regards to trajectory characteristics and feasible initial condition. Lastly, a numerical example is included to verify the theoretical findings.

II. Problem Statement

This section formally describes the problem. Equations for the engagement kinematics and constraints are summarized. The problem is then formulated as finite-horizon regulation of predicted impact angle error which is defined with respect to the final flight path angle resulting from application of Pure Proportional Navigation Guidance law (PPNG).

A. Engagement Kinematics

The following assumptions are taken for simplicity of analysis.

Assumption 1 (Lag-Free Vehicle)**.**

The vehicle is a point mass that does not experience any response lag in lateral acceleration tracking.

Assumption 2 (Error-Free Measurement)**.**

The vehicle measures or receives the target position without delay and noise corrupting the signal.

Figure 1 shows the guidance geometry which specifically depicts a surface-to-surface scenario; it launches from the

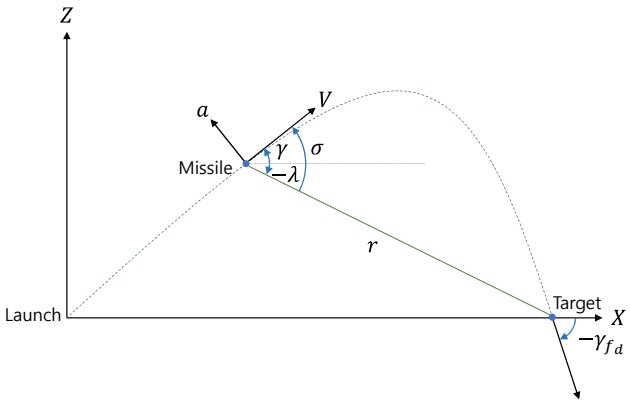


Fig. 1 Guidance Geometry

ground, raises its altitude in the midcourse stage to extend its flight range and form a desirable collision geometry. It then proceeds to the terminal homing phase. In Fig. 1, r is the range, λ denotes the line-of-sight angle, γ represents the flight path angle, and σ is the lead angle. The speed, which might be time-varying, and the lateral acceleration of the missile are represented by V and a, respectively. The angle-of-attack is neglected by Assumption 1. The lead angle σ is the angle between velocity and line-of-sight, hence, it can be considered as the look angle which is the angle between central axis of strapdown seeker and line-of-sight. The look angle is related to the other angles by

$$\sigma = \gamma - \lambda \tag{1}$$

The engagement kinematics are described by the following equations.

$$\dot{r} = -V\cos\sigma \tag{2}$$

$$\dot{\lambda} = -\frac{V}{r}\sin\sigma \tag{3}$$

$$\dot{\gamma} = \frac{a}{V} \tag{4}$$

$$\dot{\sigma} = \dot{\gamma} - \dot{\lambda} = \frac{a}{V} + \frac{V}{r}\sin\sigma \tag{5}$$

where $\dot{()} = \frac{d}{dt}()$. For a missile provided with the measurements for its speed V, line-of-sight rate $\dot{\lambda}$, and look angle σ, a pseudo-measurement for the range can be obtained by inverting Eq. (3) as $\hat{r} = -\frac{V\sin\sigma}{\dot{\lambda}}$. In the interception of a stationary target, this pseudo-range information can be used to implement a range-dependent feedback guidance law.

B. Terminal and Path Constraints

This study considers two additional constraints besides nullification of the miss distance: i) enforcement of desired impact angle, and ii) maintaining look angle within the given limit. Let t_0 and t_f denote the initial time and the final time, respectively. Additionally, let γ_{f_d} and σ_{lim} denote the desired impact angle and the maximum look angle, respectively.

The conditions that together constitute a successful mission are summarized as follows:

Condition (1) miss distance: $r \to 0$ as $t \to t_f$

Condition (2) impact angle: $\gamma \to \gamma_{f_d}$ as $t \to t_f$

Condition (3) look angle: $\sigma \in [-\sigma_{\text{lim}}, \sigma_{\text{lim}}], \forall t \in \left[t_0, t_f\right]$

Assumption 3 (Acute Look Angle Limit)**.**

The look angle limit σ_{lim} is less than 90 deg since a seeker attached to the nose cannot have view towards the opposite direction of missile velocity.

C. Problem Reformulation

Various formulations and control design schemes can be adopted for impact-angle-constrained interception. One possible approach is to design a new guidance law by augmenting a baseline algorithm. This study considers the PPNG as the baseline as it guarantees satisfaction of Condition (1). The augmentation approach turns the problem into design of additional input to meet a reduced number of conditions.

The PPNG establishes a differential relation between the flight path angle γ with the look angle σ as

$$\dot{\gamma} = N\dot{\lambda} = \frac{N}{N-1}\dot{\sigma} \tag{6}$$

where $N > 1$ is the navigation constant. By integrating both sides of Eq. (6) from the current time t to the final time t_f, the final flight path angle predicted at the current time assuming application of the PPNG can be obtained as

$$\hat{\gamma}_{f_{PPNG}}(t) = \gamma(t) - \frac{N}{N-1}\sigma(t) = \frac{N\lambda(t) - \gamma(t)}{N-1} \tag{7}$$

Note that the property $\sigma\left(t_f\right) = 0$ is used in the derivation of Eq. (7).

The impact angle error can be defined with respect to the predicted final flight path angle $\hat{\gamma}_{f_{PPNG}}$ as follows:

$$e_{\gamma_f}(t) \triangleq \hat{\gamma}_{f_{PPNG}}(t) - \gamma_{f_d} \tag{8}$$

The definition given by Eq. (8) is a natural choice to represent Condition (2) considering the existence of the baseline, because $e_{\gamma_f} = 0$ implies that a vehicle will achieve desired impact angle with no additional input.

Let us now define a new state variable $\eta \triangleq \sin\sigma$. The range r is monotonically decreasing with respect to the time t under Assumption 3 when Condition (3) is not violated. By changing the independent variable from t to r, the dynamics of the new state variable and the impact angle error can be represented as

$$\eta' = -\frac{\eta}{r} + u\sqrt{1-\eta^2} \tag{9}$$

$$e_{\gamma_f}{}' = \frac{N\lambda' - u}{N-1} \tag{10}$$

where $()' = \frac{d}{dr}()$ and $u \triangleq \gamma' = -\frac{a}{V^2\sqrt{1-\eta^2}}$ is the input variable. Let the baseline command and the bias command constitute the input as

$$u \triangleq u_{\text{base}} + u_{\text{aug}} = N\lambda' + u_{\text{aug}} = N\frac{\eta}{r\sqrt{1-\eta^2}} + u_{\text{aug}} \tag{11}$$

By substituting Eq. (11) into Eqs. (9) and (10), evolution of the new state and the impact angle error with respect to the range can be rewritten as

$$\eta' = (N-1)\frac{\eta}{r} + \sqrt{1-\eta^2}\, u_{\text{aug}} \tag{12}$$

$$e_{\gamma_f}{}' = -\frac{u_{\text{aug}}}{N-1} \tag{13}$$

It can be noticed from Eq. (13) that $e_{\gamma_f}{}'$ is linear with respect to u_{aug}.

Let $\eta_{\text{lim}} \triangleq \sin\sigma_{\text{lim}}$. The transformed problem is to design u_{aug} to satisfy the following constraints:

$$\lim_{r\to 0}\eta = 0 \tag{14}$$

$$\lim_{r\to 0} e_{\gamma_f} = 0 \tag{15}$$

$$\eta \in [-\eta_{\text{lim}}, \eta_{\text{lim}}], \forall r \in [0, r_0] \tag{16}$$

where $r_0 = r(t_0)$.

Equation (16) is valid if $|\eta|$ always shrinks or vanishes at the boundary of the constraint set, rendering $[-\eta_{\text{lim}}, \eta_{\text{lim}}]$ a forward invariant set of $\eta(r)$. That is, Eq. (16) holds if the following is true.

$$\left.\frac{d\left(\frac{1}{2}\eta^2\right)}{dr}\right|_{|\eta|=\eta_{\text{lim}}} = [\eta\eta']|_{\eta=\pm\eta_{\text{lim}}} \geq 0 \tag{17}$$

III. Linear Feedback Bias Command

This section presents nonlinear analysis of the bias command given by a linear feedback of the impact angle error. The design approach is to meet the constraints with appropriate construction of the gain functions. A sufficient condition for feasibility with respect to the impact angle and look angle constraints is presented as one of the main novelties of this study. The practical value of the proposed condition is a characterization of the feasible launch conditions or the achievable impact conditions.

A. Design of Bias Command

Considering that $e_{\gamma_f}{}'$ depends linearly on u_{aug}, as shown in Eq. (13), the bias command is proposed to have the following form,

$$u_{\text{aug}} = -\frac{K(r,\eta)}{r} e_{\gamma_f} \tag{18}$$

where $K(r,\eta) > 0$ is the variable gain. To simplify subsequent analyses and response shaping, this study considers the gain function K can be factorized as follows:

$$K(r,\eta) = K_r(r)\, K_\eta(\eta) \tag{19}$$

where $K_r(r)$ and $K_\eta(\eta)$ are the range-dependent gain and look-angle-dependent gain, respectively. In this study, it is assumed that both functions are continuous and attain strictly positive values. The function $K_\eta(\eta)$ is chosen to be an even function for simplicity of subsequent analyses. This simplification is reasonable because a symmetric look angle limit is also considered in this study. Furthermore, we can presume without loss of generality that

$$K_\eta(\eta) \geq 1, \ \forall \eta \in [-\eta_{\text{lim}}, \eta_{\text{lim}}] \tag{20}$$

because the factorization shown in Eq. (19) allows one to arbitrarily choose the lower bound of $K_\eta(\eta)$ through adjusting the value of $K_r(r)$. The factored form of Eq. (19) is chosen to allow gain shaping with respect to both the range r and the look angle σ in a decomposed manner. The range-dependence is quite natural since it is the independent variable of Eq. (13). The look-angle-dependent factor is introduced to modify the gain further in consideration of the field-of-view constraint.

B. Analysis of Impact Angle Error Convergence and Bias Command Behavior

The closed-loop system dynamics formed by the proposed bias command are given by substituting Eqs. (18) and (19) into Eqs. (12) and (13) as follows:

$$\eta' = (N-1)\frac{\eta}{r}\left[1 - \frac{\sqrt{1-\eta^2}}{(N-1)\,\eta} K_r(r)\, K_\eta(\eta)\, e_{\gamma_f}\right] \tag{21}$$

$$e_{\gamma_f}{}' = \frac{K_r(r)\, K_\eta(\eta)}{(N-1)\, r} e_{\gamma_f} \tag{22}$$

The proposed bias command guarantees exponential convergence of the impact angle error towards zero at the final time if the gain functions have particular characteristics. A sufficient condition for the terminal impact angle error becoming zero is summarized in Theorem 1.

Theorem 1 (Convergence of Impact Angle Error)**.**

The impact angle error e_{γ_f} converges to zero as $r \to r_f = 0$, if the following condition holds for the gain function in Eq. (19):

$$\lim_{r \to 0} \exp\left[\int_{r_0}^{r} \frac{K_r(s)}{s} ds\right] = 0, \ \forall r_0 > 0 \tag{23}$$

Proof. See Appendix B. □

The condition given by Eq. (23) demands that $\int_{r_0}^{r} \frac{K_r(s)}{s} ds \to -\infty$ as $r \to 0$ because the integral is contained inside the exponential function of which the range is the set of positive real numbers. From this observation, the structure for the function $K_r(r)$ admissible in view of satisfying Eq. (23) can be found as in Corollary 1.

Corollary 1 (Range-Dependent Gain for Zero Final Impact Angle Error)**.**

1) (Necessary and Sufficient Condition) Let

$$K_r^* \triangleq \underset{r \in [0, r_0]}{\text{mean}} K_r(r) = \frac{1}{r_0} \int_0^{r_0} K_r(s)\, ds. \tag{24}$$

Equation (23) holds if and only if $K_r^* > 0$.

2) (A Sufficient Condition) Let $\underline{K}_r \triangleq \min_{r \in [0, r_0]} K_r(r)$. Equation (23) is satisfied if $\underline{K}_r > 0$.

Proof. See Appendix C. □

The boundedness of the bias command throughout the engagement should be guaranteed since a command escaping to infinity incurs many instability phenomena. In fact, it is of practical interest to nullify the final value of the bias command for the missile to end the engagement with the baseline PPNG, while demonstrating a stable response and maintaining enough control authority. Corollary 2 summarizes the relevant discussions.

Corollary 2 (Range-Dependent Gain for Zero Final Value of Bias Command)**.**
If $\frac{K_r(r)}{r} \exp\left[\frac{1}{N-1} \int_{r_0}^{r} \frac{K_r(s)}{s} ds\right]$ remains bounded for $\forall r \in [0, r_0]$, then $\left|u_{\text{aug}}\right|$ is bounded from above. A stronger requirement $u_{\text{aug}}(r_f) = 0$ is satisfied, if

$$\frac{K_r(r)}{r} \exp\left[\frac{1}{N-1} \int_{r_0}^{r} \frac{K_r(s)}{s} ds\right]\Bigg|_{r=0} = 0, \ \forall r_0 > 0 \tag{25}$$

Moreover, the following conditions give a guideline for choosing $K_r(r)$ in consideration of Eq. (25). Suppose that K_r^* and $\underline{K}_r$ are defined as described in Corollary 1.

1) (Necessary and Sufficient Condition) Equation (25) holds if and only if

$$K_r^* > N - 1 \tag{26}$$

2) (A Sufficient Condition) Equation (25) is satisfied if

$$\underline{K}_r > N - 1 \tag{27}$$

Proof. See Appendix D □

Remark 1 (Indirect Design of Range-Dependent Gain Considering Prescribed Impact Angle Error Bound)**.** The proof of Theorem 1 suggests through Eq. (B.5) that one can obtain $K_r(r)$ indirectly from a prescribed bound for the impact angle error e_{γ_f}. Let the bounding function be defined by the term on the right-hand side of Eq. (B.5) as

$$\overline{e}(r) \triangleq \left|e_{\gamma_{f_0}}\right| \exp\left[\frac{1}{N-1}\int_{r_0}^{r} \frac{K_r(s)}{s} ds\right] \tag{28}$$

Provided that $\overline{e}(r)$ is given a priori as a function such that $\overline{e}(r=0) = 0$, the corresponding $K_r(r)$ can be obtained as

$$K_r(r) = (N-1)\, r \frac{\overline{e}'(r)}{\overline{e}(r)} \tag{29}$$

Using the shaping function of Eq. (29) guarantees $\left|e_{\gamma_f}(r)\right| \leq \overline{e}(r),\ \forall r \in [0, r_0]$.

C. Analysis of Look Angle Convergence

Convergence of the look angle to zero at the end of engagement is an essential requirement for accurate interception of a stationary target. Missile trajectories will show nonzero miss distance unless the final look angle is zero. Theorem 2 discusses the look angle convergence characteristics of the proposed guidance law.

Theorem 2 (Convergence of Look Angle)**.** Suppose that the look-angle-dependent gain $K_\eta(\eta)$ is upper bounded and let

$$\overline{K}_\eta \triangleq \max_{\eta \in [-\eta_{\lim}, \eta_{\lim}]} K_\eta(\eta) \tag{30}$$

denote the finite maximum value. In addition, suppose that $\overline{K}_\eta \geq 1$ for the given $K_\eta(\eta)$ so that it is consistent with Eq. (20), i.e.,

$$1 \leq K_\eta(\eta) \leq \overline{K}_\eta < \infty,\ \forall \eta \in [-\eta_{\lim}, \eta_{\lim}] \tag{31}$$

The proposed non-switching guidance law ensures that the look angle converges to zero as represented by Eq. (14).

Proof. See Appendix E. □

D. Analysis of Look Angle Boundedness and Feasible Initial Conditions

The proposed bias command with properly designed gain functions can assure that the look angle is bounded below the specified maximum value. Theorem 3 summarizes the conditions that should be satisfied by the gain functions in order for the target to remain inside the seeker's field of view.

Theorem 3 (Boundedness of Look Angle)**.**
Suppose that $\eta(r_0) = \sin\sigma(t_0)$ is contained in the set $[-\eta_{\lim}, \eta_{\lim}]$. The proposed non-switching guidance law satisfies the look angle restriction represented by Eq. (16) if the following condition holds for the gains $K_r(r)$ and $K_\eta(\eta)$ in addition to Eqs. (20) and (23):

$$K_r(r)\exp\left[\frac{1}{N-1}\int_{r_0}^{r}\frac{K_r(s)}{s}ds\right] \le \frac{(N-1)\tan\sigma_{\lim}}{\left|e_{\gamma_{f_0}}\right| K_{\eta_{\lim}}} \tag{32}$$

where $K_{\eta_{\lim}} = K_\eta(\pm\eta_{\lim})$.

Proof. See Appendix F. □

Remark 2 (Indirect Design of Range-Dependent Gain Considering Look Angle Boundedness)**.**
One possible design approach that considers compliance with Eq. (32) is to specify the function on the LHS as a desired form instead of choosing the function $K_r(r)$ itself. For convenience, let us define a new function as $G(r) \triangleq K_r(r)\exp\left[\frac{1}{N-1}\int_{r_0}^{r}\frac{K_r(s)}{s}ds\right]$. Note that $G(r_0) = K_r(r_0)$. Differentiating the relation with respect to r results in

$$\begin{aligned} G'(r) &= \left\{K_r{}'(r) + \frac{K_r{}^2(r)}{(N-1)\,r}\right\}\exp\left[\frac{1}{N-1}\int_{r_0}^{r}\frac{K_r(s)}{s}ds\right] \\ &= \left\{\frac{K_r{}'(r)}{K_r(r)} + \frac{K_r(r)}{(N-1)\,r}\right\}G(r) \end{aligned} \tag{33}$$

Equation (33) can be rewritten as follows:

$$K_r'(r) - \frac{G'(r)}{G(r)}K_r(r) = -\frac{1}{(N-1)\,r}K_r{}^2(r) \tag{34}$$

Provided that the desired $G(r)$ is determined, the range-dependent gain $K_r(r)$ can be obtained by solving Eq. (34), which is a Bernoulli differential equation [26]. By utilizing the simple transformation $w = K_r{}^{-1}$, the solution for Eq. (34) can be easily derived in closed form as

$$K_r(r) = \frac{G(r)}{1 + \int_{r_0}^{r}\frac{G(s)}{(N-1)s}ds} \tag{35}$$

The proposed nonlinear bias shaping method yields accurate miss distance and impact angle performance without violation of the look angle inequality. However, the look angle limit and the vehicle maneuverability should be

sufficiently large to achieve impact angles of higher magnitudes. That is, the achievable impact angles or, alternatively, the feasible launch angles are restricted by the greatest possible values of both look angle and lateral acceleration. The set of feasible initial conditions that always results in a successful impact-angle-constrained interception and a magnitude of the look angle less than or equal to the limit value can be derived as a direct corollary of Theorem 3.

Corollary 3 (Set of Feasible Initial Conditions)**.**

Let $\overline{K}_r \triangleq \max_{r\in[0,r_0]} K_r(r)$. The look angle restriction represented by Eq. (16) is guaranteed if the initial condition satisfies the following inequality:

$$\left|e_{\gamma_{f_0}}\right| \leq \frac{(N-1)\tan\sigma_{\lim}}{\overline{K}_r K_{\eta_{\lim}}} \tag{36}$$

Furthermore, in the particular scenario of ground-to-ground engagement where $\gamma_0 = \sigma_0 > 0$ and $\gamma_{f_d} < 0$, Eq. (36) specifies the feasible range of the launch angle γ_0 for a fixed desired impact angle γ_{f_d} as follows:

$$-(N-1)\left\{\frac{(N-1)\tan\sigma_{\lim}}{\overline{K}_r K_{\eta_{\lim}}} + \gamma_{f_d}\right\} \leq \gamma_0 \leq (N-1)\left\{\frac{(N-1)\tan\sigma_{\lim}}{\overline{K}_r K_{\eta_{\lim}}} - \gamma_{f_d}\right\} \tag{37}$$

Conversely, the feasible set of γ_{f_d} for a fixed γ_0 is

$$-\frac{(N-1)\tan\sigma_{\lim}}{\overline{K}_r K_{\eta_{\lim}}} - \frac{\gamma_0}{N-1} \leq \gamma_{f_d} \leq \frac{(N-1)\tan\sigma_{\lim}}{\overline{K}_r K_{\eta_{\lim}}} - \frac{\gamma_0}{N-1} \tag{38}$$

Proof. See Appendix G. □

Remark 3 (Choice of Gains Resulting in the Widest Set of Feasible Initial Conditions)**.**

Limitations in the region of initial conditions restrict the practicable mission plan and bring the necessity to set the launch angle precisely. One desirable direction in the design and implementation of a guidance law is to provide the maximum possible flexibility in the applicable engagement geometries. It can be observed from Corollary 3 that a lower $\overline{K}_r K_{\eta_{\lim}}$ value results in a wider allowable range of $e_{\gamma_{f_0}}$. In this regard, one may attain the largest set of feasible initial conditions by choosing $\overline{K}_r K_{\eta_{\lim}}$ as small as possible. A practical guideline for tuning of the gains can then be summarized as follows:

- The possible minimum value of $K_{\eta_{\lim}}$ is 1 in view of Eq. (20). The even function $K_\eta(\eta)$ would be better given by a concave function satisfying $K_{\eta_{\lim}} = 1$.
- Corollary 2 shows that the choice of $K_r(r)$ should comply with Eq. (27) if the bias command is required to be zero at the final time. In this case, the possible minimum value of $\overline{K}_r$ is restricted by Eq. (27) because $\overline{K}_r \geq K_r(r) \geq \underline{K}_r > N-1$.

Putting together the discussions on gains stated above, one typical example for the gain design can be given as

$$\begin{aligned} K_r\left(r\right) &= N-1+\delta \\ K_\eta\left(\eta\right) &= 1+k\left(1-\left|\frac{\eta}{\eta_{\text{lim}}}\right|^m\right) \end{aligned} \tag{39}$$

where $\delta > 0$ is a sufficiently small constant, $k > 0$ is a constant that essentially determines $\overline{K}_\eta$, and $m > 1$ is a sufficiently large constant.

A point to note from the guideline is that if the zero final bias requirement is enforced, the range of feasible $e_{\gamma_{f_0}}$ is actually determined as a function of only the maximum look angle as

$$\left|e_{\gamma_{f_0}}\right| < \tan\sigma_{\text{lim}} \tag{40}$$

One may arrive at Eq. (40) by applying the design guideline expressions $K_{\eta_{\text{lim}}} = 1$ and $\bar{K}_r > N-1$, which are discussed in the bullet list of Remark 3, to the right-hand-side of Eq. (36). This implies that the choice of gain has no effect in enlarging the set of feasible initial conditions determined by the sufficient condition proposed in Corollary 3. The exact determination of the area of feasible initial conditions is beyond the scope of discussion based only on the sufficient condition, which in turn necessitates numerical simulations over a grid of initial conditions to completely evaluate the effect of gains.

Remark 4 (Maneuverability Limit Considerations)**.**
As discussed in the previous studies [3, 10], guidance command usually has extrema around the beginning of flight and the instance at which the bias command is nullified. The bias command dominates the baseline PPNG command in the initial moment due to the large initial impact angle error and the negligible line-of-sight rate for a large initial range. Conversely, the baseline PPNG command dominates the bias command as the engagement comes closer to the end under the assumption that the impact angle error converges to zero rapidly. In these respects, the maximum command that appears at the beginning of flight and the instance of achieving zero e_{γ_f} can be approximated, respectively, by using Eqs. (D.1) and (32) as

$$\begin{aligned} \max_{r\in[r_s,r_0]}\left|u\left(r\right)\right| &\approx \frac{K_r\left(r_0\right)K_\eta\left(\eta_0\right)}{r_0}\left|e_{\gamma_{f_0}}\right| \leq \frac{N-1}{r_0}\frac{\overline{K}_\eta}{K_{\eta_{\text{lim}}}}\tan\sigma_{\text{lim}} \\ \max_{r\in[0,r_s]}\left|u\left(r\right)\right| &\approx N\frac{\tan\sigma_{\text{lim}}}{r_s} \end{aligned} \tag{41}$$

where r_s is the settling range such that $\left|e_{\gamma_f}\left(r\right)\right| \leq \varepsilon\left|e_{\gamma_{f_0}}\right|$ for $r \leq r_s$ with a small positive constant $\varepsilon \ll 1$. If $K_r\left(r\right)$ is simply chosen as a constant greater than $N-1$, Eq. (B.5) becomes $\left|e_{\gamma_f}\left(r\right)\right| \leq \left|e_{\gamma_{f_0}}\right|\left(\frac{r}{r_0}\right)^{\frac{K_r}{N-1}}$; therefore, the settling range for this case can be obtained by $r_s = \varepsilon^{\frac{N-1}{K_r}}r_0$. This relation shows that a larger constant K_r results in a larger r_s. It can then be inferred from Eq. (41) that if all the other design parameters and initial conditions are not altered, a

larger value for the constant K_r may reduce the maximum command during the mission but only at the expense of an increased maximum command in the initial phase. One might choose the constant K_r for the extreme command values of both phases not to exceed a certain limit, while obeying other conditions such as that for impact angle convergence. As explained in the example of choosing $K_r\,(r)$ as a constant, the value of gains and the set of feasible initial conditions are further affected by the maneuverability limit constraint $|u\,(r)| \leq u_{\max}$ through Eq. (41). Note that $\overline{K}_\eta$ might be chosen to be consistent with a given maneuverability limit.

Remark 5 (Comparison with Earlier Result on Feasible Initial Conditions)**.**
A sophisticated design of the bias command to meet similar design objectives was presented in [3] together with an approximate but practically valuable analysis. The analysis on the achievable maximum impact angle presented in [3] assumed $\sigma_0 = \gamma_0 = \sigma_{\lim}$ to make the engagement consist of two guidance phases instead of three. The feasible maximum magnitude of γ_{f_d} is obtained by three distinct conditions. The conditions governing the set of achievable impact angles were 1) the existence of the switching point represented in terms of the range being positive, 2) the sufficiency of the terminal phase duration for settling of the impact angle error, and 3) the acceleration command being less than the vehicle's maneuverability limit.

The criteria considered in the analysis of [3] are different from the conditions taken into consideration in the investigation of feasible initial conditions for the nonlinear guidance law proposed in this study. The analysis of the earlier study was performed in consideration of the missile maneuverability limit, while the proposed study considered nullification of the bias command. However, the analysis in [3] involves numerical computations to test whether each of the criteria is satisfied or violated. As a consequence, the result of the previous study is useful for estimating the feasibility of a given initial condition but not for the inverse process, i.e., analytical determination of the feasible initial condition boundaries.

IV. Fractional Power Feedback Bias Command

This section discusses the design and analysis of a bias command for the same guidance objectives as those in the previous section, but takes a different structure for the bias command. This section describes one particular type of fractional power feedback unlike the linear feedback, described in Sec. III: a bias command comprised of the impact angle taken to a fractional power and multiplied by a variable gain. The analyses presented in Sec. III are performed in a similar fashion for the fractional power feedback guidance law. The purpose is to show how the analytical results on the convergence and boundedness characteristics and the set of feasible initial conditions change depending on the command structure.

A. Design of Bias Command and Analysis of Impact Angle Error Convergence

The bias command for the finite-horizon regulation of the error can also be proposed as follows:

$$u_{\text{aug}} = -\frac{K_r(r)\,K_\eta(\eta)}{r}\left|e_{\gamma_f}\right|^p \operatorname{sgn}\left(e_{\gamma_f}\right), \quad p \in (0,1) \tag{42}$$

The bias command given by Eq. (42) is clearly nonlinear in e_{γ_f}, whereas the bias command of the previous section, Eq. (18), has the form of linear feedback of e_{γ_f}. $K_r(r)$ and $K_\eta(\eta)$ are again the variable gains.

The closed-loop system dynamics formed by the proposed nonlinear error feedback bias command is given by substituting Eqs. (42) into Eqs. (12) and (13) as follows:

$$\eta' = (N-1)\frac{\eta}{r}\left[1 - \frac{\sqrt{1-\eta^2}}{(N-1)\,\eta}K_r(r)\,K_\eta(\eta)\left|e_{\gamma_f}\right|^p \operatorname{sgn}\left(e_{\gamma_f}\right)\right] \tag{43}$$

$$e_{\gamma_f}{}' = \frac{K_r(r)\,K_\eta(\eta)}{(N-1)\,r}\left|e_{\gamma_f}\right|^p \operatorname{sgn}\left(e_{\gamma_f}\right) \tag{44}$$

The proposed fractional power feedback bias command can guarantee the convergence of the impact angle error before interception, as shown in Theorem 4.

Theorem 4 (Convergence of Impact Angle Error Before Interception)**.**
The impact angle error e_{γ_f} converges to zero before interception with the nonlinear error feedback bias command of Eq. (42) if Eq. (20) and the following condition are satisfied:

$$\lim_{r\to 0}\int_{r_0}^{r}\frac{K_r(s)}{s}ds < -\frac{N-1}{1-p}\left|e_{\gamma_{f_0}}\right|^{1-p} \tag{45}$$

Proof. See Appendix H. □

B. Analysis of Look Angle Boundedness and Feasible Initial Conditions

The boundedness of look angle below the given limit can also be guaranteed for the fractional power feedback bias command with a proper gain function. By closely following a similar reasoning as the previous section, required conditions can be derived as summarized in Theorem 5.

Theorem 5 (Boundedness of Look Angle)**.**
Suppose that $\eta(r_0) = \sin\sigma(t_0)$ is contained in the set $[-\eta_{\lim}, \eta_{\lim}]$. The nonlinear error feedback bias command of Eq. (42) satisfies the look angle restriction represented by Eq. (16) if the following condition holds for the gains $K_r(r)$ and $K_\eta(\eta)$ in addition to Eqs. (20) and (45).

$$K_r(r)\left[\left|e_{\gamma_{f_0}}\right|^{1-p} + \frac{1-p}{N-1}\int_{r_0}^{r}\frac{K_r(s)}{s}ds\right]^{\frac{p}{1-p}} \le \frac{(N-1)\tan\sigma_{\lim}}{K_{\eta_{\lim}}}, \quad \forall r \in [r^*, r_0] \tag{46}$$

Proof. See Appendix I. □

The set of feasible initial conditions for the fractional power feedback bias command can also be obtained as a direct consequence of Theorem 5.

Corollary 4 (Set of Feasible Initial Conditions)**.**
When the fractional power feedback bias command of Eq. (42) is used, the initial condition lying in the set bounded by the following inequality is sufficient for guaranteeing the look angle restriction represented by Eq. (16):

$$\left|e_{\gamma_{f_0}}\right|^p \leq \frac{(N-1)\tan\sigma_{\lim}}{\overline{K}_r K_{\eta_{\lim}}} \tag{47}$$

Proof. See Appendix J. □

Remark 6 (Comparison Between Linear Feedback and Fractional Power Feedback)**.**
Let $u_{\text{aug}}^{\text{L}}$ and $u_{\text{aug}}^{\text{F}}$ denote the bias commands of linear feedback form given by Eq. (18) and fractional power feedback form given by Eq. (42), respectively. Then, the different forms are related to each other as follows:

$$u_{\text{aug}}^{\text{F}} = k\left(e_{\gamma_f}\right) u_{\text{aug}}^{\text{L}} \tag{48}$$

where $k\left(e_{\gamma_f}\right) \triangleq \left|e_{\gamma_f}\right|^{p-1}$ with $0 < p < 1$. One might understand Eq. (48) from the perspective that an additional element $k\left(e_{\gamma_f}\right)$ contained in the gain turns the linear feedback command into the fractional power feedback command. Because $k\left(e_{\gamma_f}\right) \leq 1$ for $\left|e_{\gamma_f}\right| \geq 1$, and $k\left(e_{\gamma_f}\right) \geq 1$ for $\left|e_{\gamma_f}\right| \leq 1$, it is clear from the relation that

$$\begin{aligned} \left|u_{\text{aug}}^{\text{F}}\right| &\leq \left|u_{\text{aug}}^{\text{L}}\right| \quad \text{for} \quad \left|e_{\gamma_f}\right| \geq 1 \\ \left|u_{\text{aug}}^{\text{F}}\right| &\geq \left|u_{\text{aug}}^{\text{L}}\right| \quad \text{for} \quad \left|e_{\gamma_f}\right| \leq 1 \end{aligned} \tag{49}$$

The physical interpretation for Eq. (49) is that as a consequence of employing $k\left(e_{\gamma_f}\right)$, the fractional power structure reduces control action for large errors and amplifies control action for small errors. The convergence of the impact angle at a nonzero range, i.e., before interception, shown for the fractional power feedback case in Theorem 4 is attributed to this control action amplification behavior.

The bias command structure also affects the set of feasible initial conditions characterized by the sufficiency sense in Corollary 3 and Corollary 4 for $u_{\text{aug}}^{\text{L}}$ and $u_{\text{aug}}^{\text{F}}$, respectively. Let C denote the common right-hand sides of Eqs. (36) and (47). Then, the upper bounds on $\left|e_{\gamma_{f_0}}\right|$ for $u_{\text{aug}}^{\text{L}}$ and $u_{\text{aug}}^{\text{F}}$ can be represented as C and $C^{\frac{1}{p}}$, respectively. Because $0 < p < 1$, $C^{\frac{1}{p}} \geq C$ if $C \geq 1$, and $C^{\frac{1}{p}} \leq C$ if $C \leq 1$. This implies that the relative difference between the bounds on the initial condition for the different command types depends on whether C exceeds 1 or not. The fractional power

feedback places a more restrictive bound on the initial condition when compared to the linear feedback if $C \leq 1$.

V. Numerical Simulation

This section presents numerical examples to illustrate the trajectory characteristics of the BPNG investigated in the previous sections. Readers are referred to Appendix A for the batch simulation performed to verify the theoretical analysis on the range of feasible engagement conditions against the numerical experiment. Comparison with other guidance laws developed for the same problem is not included here, but interested readers may refer to the precursor of this study, [16], for the comparative simulation. All simulations are performed using the simple dynamic model consisting of the point-mass kinematics and the first-order lag model for the acceleration tracking response with time as the independent variable. A saturation function is applied to limit the acceleration command within certain bound, thus the simulation model can be summarized as

$$\begin{aligned} \dot{x} &= V\cos\gamma \qquad & \dot{y} &= V\sin\gamma \\ \dot{\gamma} &= \frac{a}{V} & \dot{a} &= \frac{\text{sat}\left(a_{cmd}, a_{\max}\right) - a}{\tau_a} \end{aligned} \tag{50}$$

where $\text{sat}\left(x, x_{\max}\right) \triangleq \min\left(\max\left(x, -x_{\max}\right), x_{\max}\right)$ for a threshold value $x_{\max} > 0$. The linear feedback command given by Eq. (18) is treated here as a special case of the fractional power feedback command given by Eq. (42) with $p = 1$. The bias gain functions $K_r\left(r\right)$ and $K_\eta\left(\eta\right)$ are chosen in a way extending Eq. (39) as

$$\begin{aligned} K_r\left(r\right) &= \left(N - 1 + \delta\right)\left(1 + \frac{r}{r_0}\right)^n \\ K_\eta\left(\eta\right) &= 1 + k\left(1 - \left|\frac{\eta}{\eta_{\text{lim}}}\right|^m\right) = 1 + k\left(1 - \left|\frac{\sin\sigma}{\sin\sigma_{\text{lim}}}\right|^m\right) \end{aligned} \tag{51}$$

where $\delta > 0$ is a sufficiently small constant, $n \geq 0$ is a constant that essentially determines $\overline{K}_r$, $k > 0$ is a constant that essentially determines $\overline{K}_\eta$, and $m > 1$ is a sufficiently large constant. Note that $\overline{K}_r = 2^n\left(N - 1 + \delta\right)$ increases with greater n, and $K_{\eta_{\text{lim}}} = 1$. Combining the definition of control input u in Eq. (11), the relation between u and a_{cmd}, and the gain functions in Eq. (51), the lateral acceleration command equation used for simulating the BPNG can be summarized as

$$a_{cmd} = NV\dot{\lambda} + \frac{\left(N - 1 + \delta\right)V^2}{r}\left(1 + \frac{r}{r_0}\right)^n \cos\sigma\left[1 + k\left(1 - \left|\frac{\sin\sigma}{\sin\sigma_{\text{lim}}}\right|^m\right)\right]\left|e_{\gamma_f}\right|^p \text{sgn}\left(e_{\gamma_f}\right), \quad p \in (0, 1] \tag{52}$$

where the expressions for $\dot{\lambda}$ and e_{γ_f} are given in Eqs. (3) and (8), respectively.

Simulation cases are divided into two different scenarios to show the effect of the design parameters (p, n) on the closed-loop trajectories. Case 1 shows the examples for the guidance law with different p and fixed n, whereas Case 2

presents the examples with identical setup except considering fixed p and different n instead. The simulation parameters for each case are summarized in Table 1. Note that the result for $p = 1$ in Case 1 corresponds to the linear feedback command. Also note that the pair (γ_0, γ_{f_d}) is chosen so that it satisfies the sufficient condition for constraint feasibility given by Eq. (A.1) for every combination (p, n) considered for trajectory demonstration.

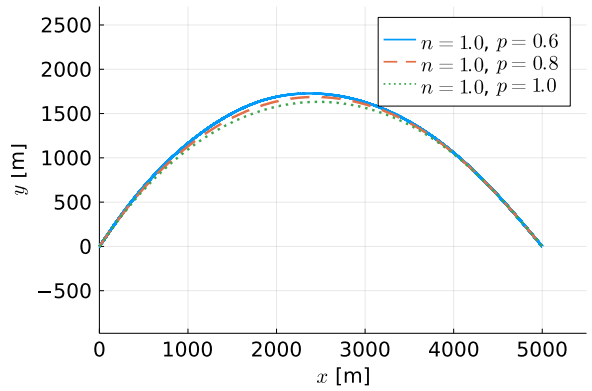
Table 1 Simulation Parameters

Parameter	Symbol	Case 1	Case 2	Appendix A
Initial Range and LOS angle	(r_0, λ_0)	(5 000 m, 0 deg)	(5 000 m, 0 deg)	(5 000 m, 0 deg)
Initial Flight Path Angle	γ_0	55 deg	55 deg	$\{0 : 5 : 60\}$ deg
Speed of Missile	V	300 m/s	300 m/s	300 m/s
Acceleration Tracking Time Constant	τ_a	0.01 s	0.01 s	–
Maximum Acceleration	$a_{\max}$	300 m/s^2	300 m/s^2	300 m/s^2
Look Angle Limit	$\sigma_{\lim}$	60 deg	60 deg	60 deg
Desired Impact Angle	γ_{f_d}	−50 deg	−50 deg	$\{-180 : 5 : 0\}$ deg
Navigation Constant	N	3	3	3
Parameters for K_r (r)	n	1	$\{0, 1, 2\}$	$\{0, 1, 3\}$
	δ	0.01	0.01	0.01
Parameters for K_η (η)	k	4	4	4
	m	10	10	10
Exponents for Fractional Power Feedback	p	$\{0.6, 1\}$	0.9	$\{0.6, 0.8, 1\}$

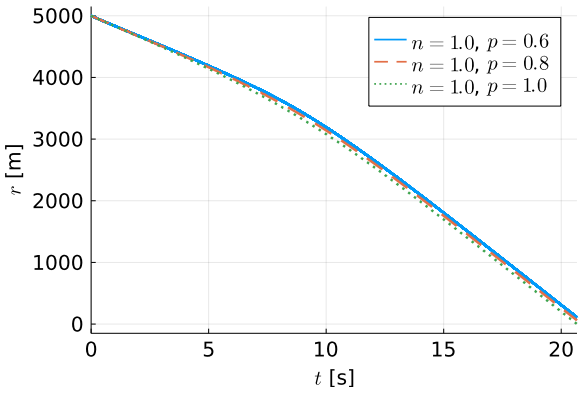
Figures 2 and 3 show the results for Case 1 and Case 2, respectively, with a fixed pair of initial and final conditions (γ_0, γ_{f_d}) and various combinations of design parameters (p, n). Figures 2(c), 2(d), 3(c), and 3(d) show that the generalized BPNG based on fractional power feedback with design parameters in the feasible range for the given (γ_0, γ_{f_d}) provides satisfactory performance. The guidance law achieves interception with the desired impact angle while satisfying the look angle constraint. The trajectories exhibit similar overall trend but show differences near the beginning of engagement depending on (p, n) (see Figs. 2(a), 2(b), 3(a), and 3(b)).

Convergence of the impact angle error is more rapid for smaller p as shown in Fig. 2(e) and for larger n as shown in Fig. 3(e). The faster response accompanies more rapid change in acceleration as shown in Figs. 2(f) and 3(f). The result is consistent with the discussion of Remark 6 which showed that the fractional power feedback command amplifies the action when the error is relatively small and enhances the rate of error convergence. Also, Fig. 2(f) shows that the lateral acceleration response exhibits sharper transition around the instance at which e_{γ_f} converges to zero with smaller p, since e_{γ_f} and, consequentially, a_{bias} reduces to zero more rapidly. On the other hand, Fig. 3(d) shows that a larger n achieves earlier convergence of e_{γ_f} to zero at the cost of increased look angle near the beginning of mission.

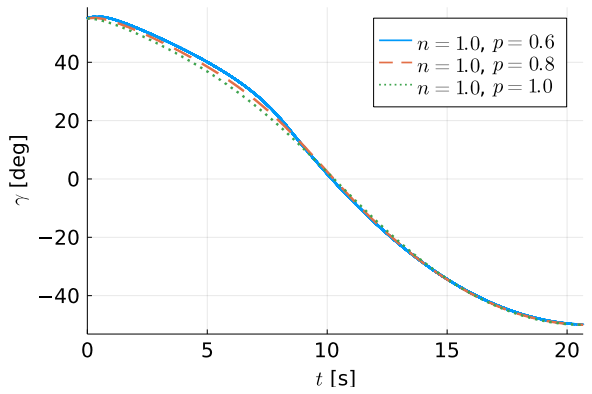
In summary, the simulation results illustrate the dependence of error convergence characteristics on the bias command design parameters p and n and also support the analytical findings discussed in Secs. III and IV.



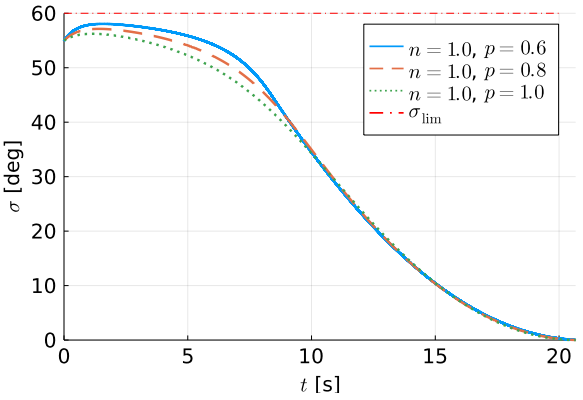
(a) Trajectories



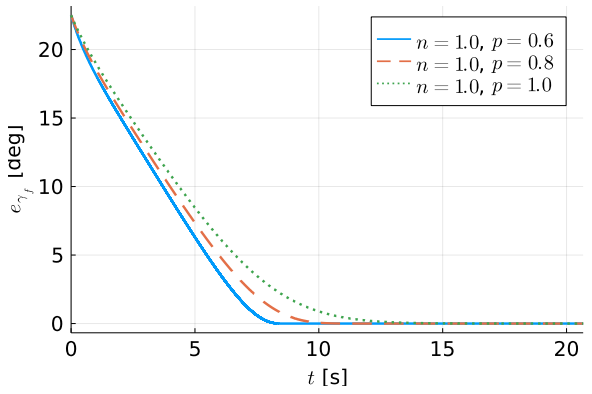
(b) Range



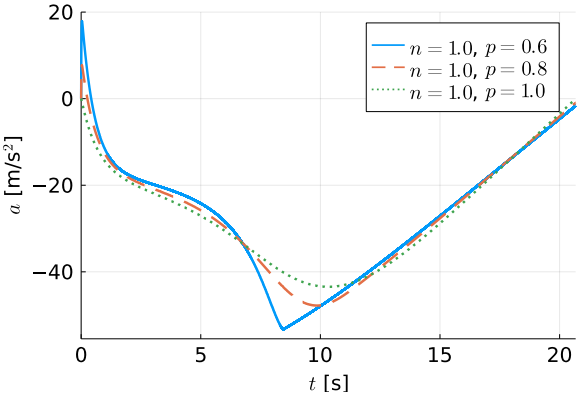
(c) Flight Path Angle



(d) Look Angle

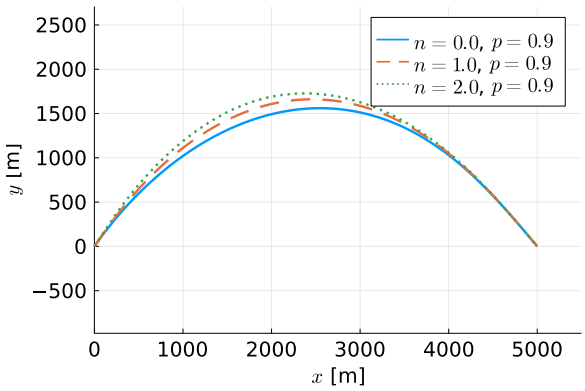


(e) Impact Angle Error

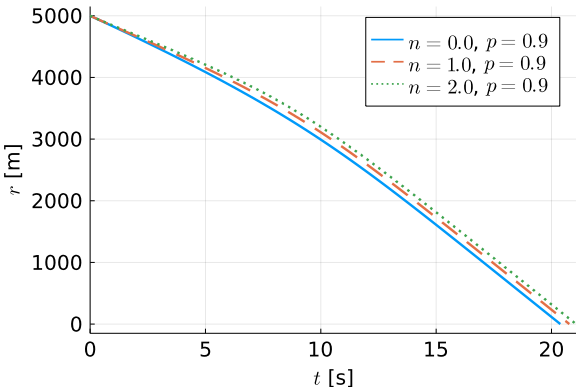


(f) Acceleration

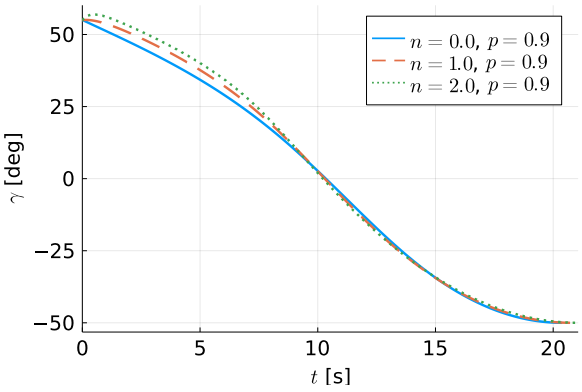
Fig. 2 Simulation Results for Case 1 - Various p, Fixed n



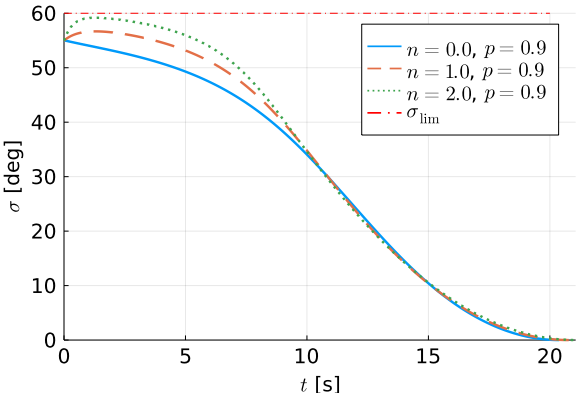
(a) Trajectories



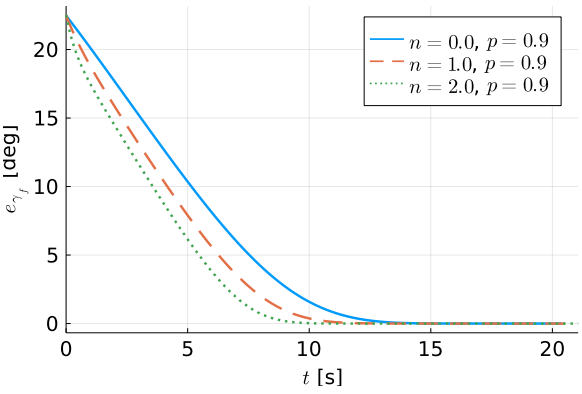
(b) Range



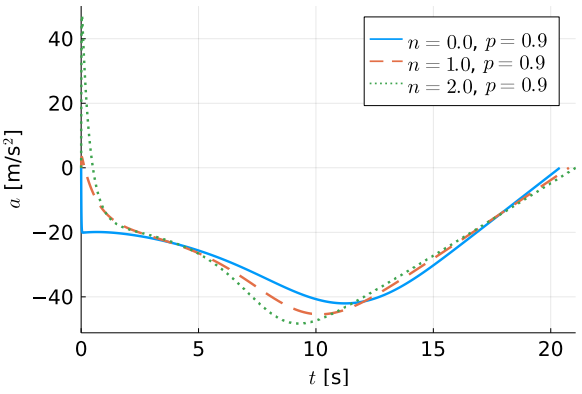
(c) Flight Path Angle



(d) Look Angle



(e) Impact Angle Error



(f) Acceleration

Fig. 3 Simulation Results for Case 2 - Fixed p, Various n

VI. Conclusions

This study carried out a generalized analysis of biased proportional navigation guidance laws with variable gain for stationary target interception with a desired impact angle while maintaining look angle in a limited range. The analysis focused on clarifying the criteria for designing the bias gain as a smooth function of range and look angle to satisfy the constraints. Two different structures were considered for the bias command: the linear feedback, and the fractional power feedback. The comparison between linear and fractional power feedback bias commands showed the effect of command structure on the convergence characteristics and the range of achievable mission configurations. Also, this study provides an estimate for the set of admissible initial and final flight path angle pairs guaranteeing look angle constraint satisfaction during the engagement by investigating how the feasible initial value of impact angle error is determined by maximum look angle and bias gain function designs. Exhaustive tests based on numerical simulation over a grid of mission profiles verify the theoretical quantification of the set of feasible conditions. Overall, the analytical results of this study applies to a wide class of biased proportional navigation guidance laws, thus providing a unified framework for constructing a non-switching guidance method with appropriate design parameters to achieve desired closed-loop behaviors.

Appendix

A. Batch Simulation for Verification of Bounds for Feasible Engagement Conditions

This Appendix presents a numerical example focusing on verification of the theoretical discussions in Secs. III and IV on the feasible initial conditions for the BPNG. More specifically, this experiment performs simulation over a grid of initial flight path angle γ_0 and the desired impact angle γ_{f_d} for each combination of bias command design parameters. The batch simulation here considers the BPNG command given in Eq. (52) which is also used for trajectory demonstrations in Sec. V. A command limiter is included in the simulation model to keep the guidance command within the maximum acceleration limit, because a large command might be produced due to the large $\left|e_{\gamma_{f_0}}\right|$ around the beginning of flight. However, unlike the one used in Sec. V, the autopilot response lag effect is neglected from Eq. (50).

Corollaries 3 and 4 along with the restriction that a missile cannot attack a target from the bottom in surface-to-surface missions indicate that the set of feasible mission configurations can be estimated as

$$-\left\{\frac{(N-1)\tan\sigma_{\lim}}{\overline{K}_r K_{\eta_{\lim}}}\right\}^{\frac{1}{P}} - \frac{\gamma_0}{N-1} \leq \gamma_{f_d} \leq \min\left[0, \left\{\frac{(N-1)\tan\sigma_{\lim}}{\overline{K}_r K_{\eta_{\lim}}}\right\}^{\frac{1}{P}} - \frac{\gamma_0}{N-1}\right] \tag{A.1}$$

which is a sufficient condition for look angle constraint satisfaction; if a pair $\left(\gamma_0, \gamma_{f_d}\right)$ satisfies Eq. (A.1), then the look angle remains inside the given limit throughout the flight. One can verify Corollaries 3 and 4 by investigating whether the actual set of feasible mission configurations obtained by numerical simulation includes the entire region quantified

by Eq. (A.1).

A surface-to-surface attack scenario is considered. For each combination of design parameters (p, n), a set of numerical simulations is performed over a grid of (γ_0, γ_{f_d}). The batch simulation parameters are summarized in the last column of Table 1. The range of γ_0 being tested is chosen to satisfy the look angle constraint at the initial time. Negative values are only physically meaningful for γ_{f_d}. The simulation software utilizes multi-thread processing with Julia as the programming language. In each case, simulation is stopped whenever the look angle σ exceeds its limit σ_{lim} or the missile arrives at the target.

Figure 4 shows the indicator of successful interception distributed over the grid of (γ_0, γ_{f_d}). Figure 5 carries the similar information by showing the coloured map for the minimum range achieved before the end of simulation. Also, Figs. 6 and 7 show the two-dimensional trajectories and the look angle magnitude histories for the cases resulted in successful interception when $\gamma_0 = \sigma_{\text{lim}}$. In Fig. 4, a point marked with blue circle represents successful interception, whereas red x-shaped cross represents the case ended in failure due to look angle constraint violation. The red and green dashed lines in Fig. 4 are the lower and upper bounds for feasible γ_{f_d} as estimated by Eq. (A.1), respectively. The region between two dashed lines belong to the estimated set of feasible γ_{f_d} for each γ_0. One can observe from Fig. 4 that the estimated set of feasible mission configurations is included entirely in the actual feasible set for all (p, n) pairs. Therefore, the numerical result verifies consistency with the theoretical findings in Corollaries 3 and 4.

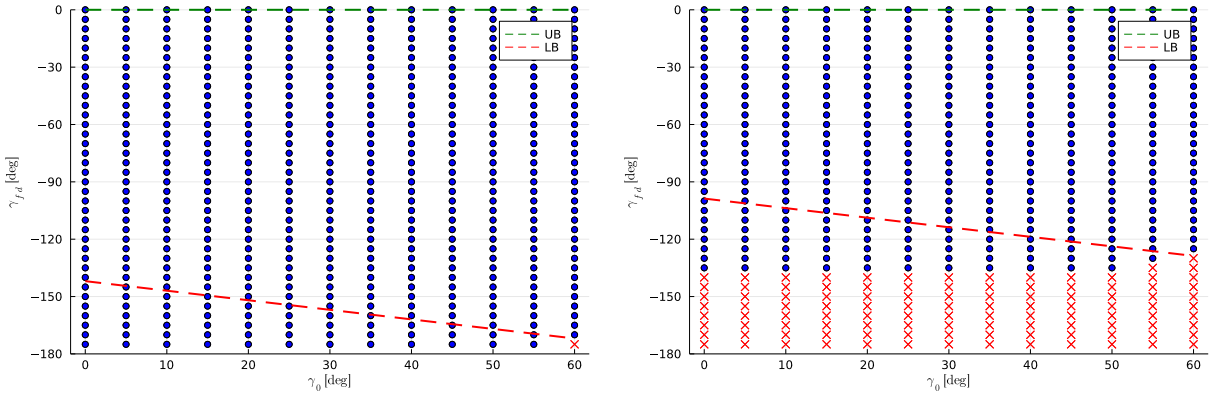
Discrepancies exist between the estimated and actual set of feasible mission configurations as shown in Fig. 4, because the bounds in Eq. (A.1) are derived as a sufficient condition for trajectory feasibility which is not necessarily an exact characterization. Nevertheless, the expressions for the bounds provide useful insights about how the actual set of feasible initial/final conditions vary depending on the design parameters, e.g., (p, n). Figure 4 shows that the area between the feasible set bounds decreases as p increases when $n = 0$, while it becomes slightly larger for greater p when $n > 0$. The observed tendency is identical to the analysis of Remark 6 stating that increasing p widens the feasible range when $\frac{(N-1)\tan\sigma_{\text{lim}}}{\overline{K}_r K_{\eta_{\text{lim}}}} \leq 1$, but otherwise an increased p reduces the feasible range.

B. Proof of Theorem 1

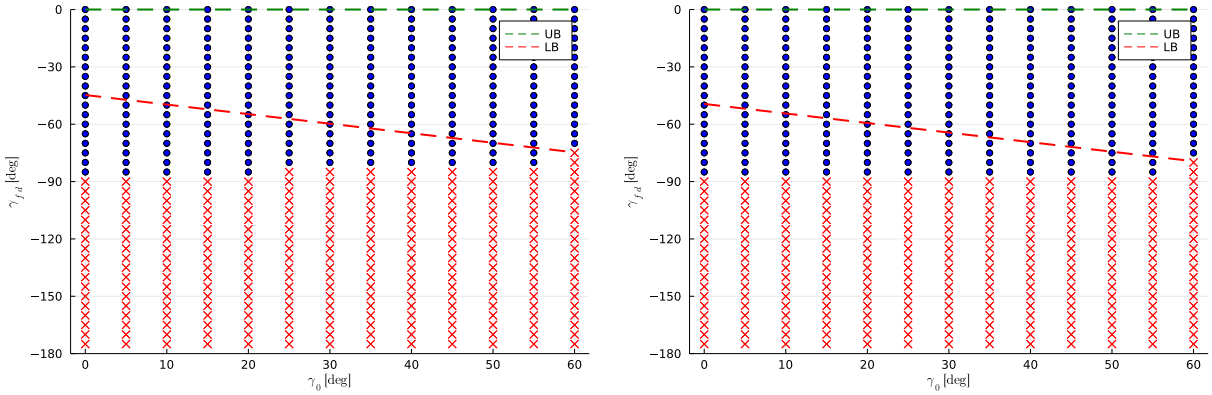
Consider the following Lyapunov candidate function for the design of u_{aug}:

$$\mathcal{V}(r) = \frac{1}{2} {e_{\gamma_f}}^2 \tag{B.1}$$

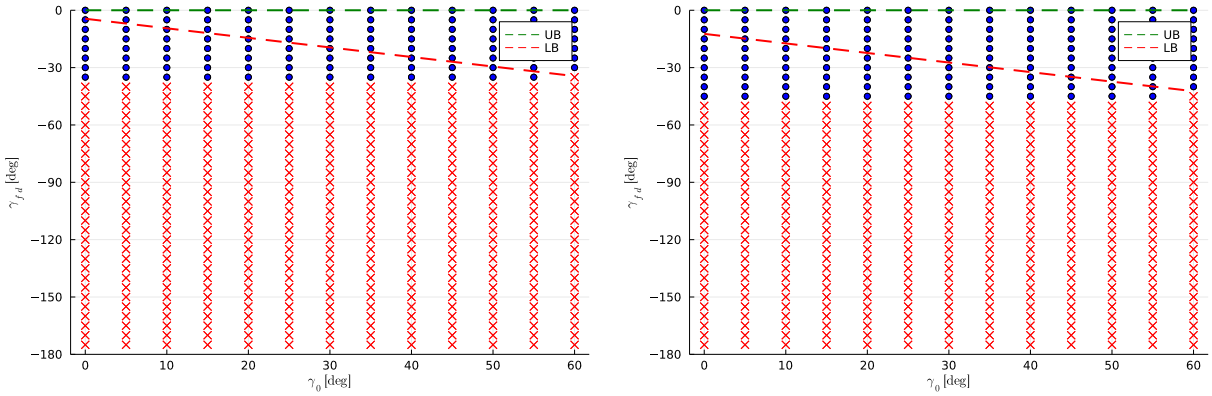
Note that $V \geq 0$, and $\mathcal{V} = 0$ if and only if $e_{\gamma_f} = 0$. The Lyapunov function $\mathcal{V}$ should be increasing with respect to r for the convergence of the impact angle error towards zero because the range r decreases with respect to time t. Using Eq.



(a) $p = 0.6, n = 0$ (b) $p = 1, n = 0$

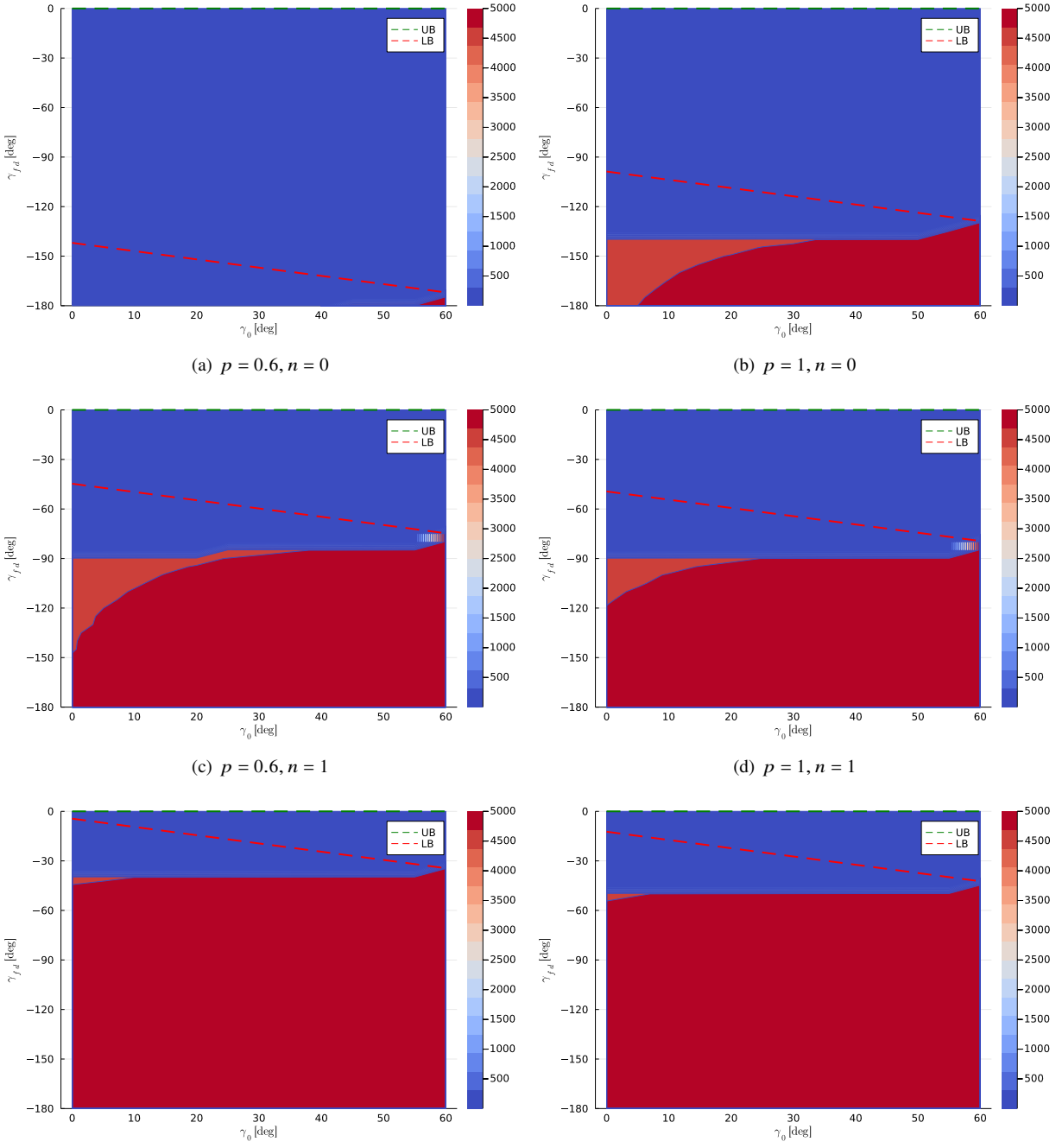


(c) $p = 0.6, n = 1$ (d) $p = 1, n = 1$



(e) $p = 0.6, n = 3$ (f) $p = 1, n = 3$

Fig. 4 Mission Accomplishment Flag and Estimated Feasible Set Boundaries for Each (γ_0, γ_{fd})



(a) $p = 0.6, n = 0$

(b) $p = 1, n = 0$

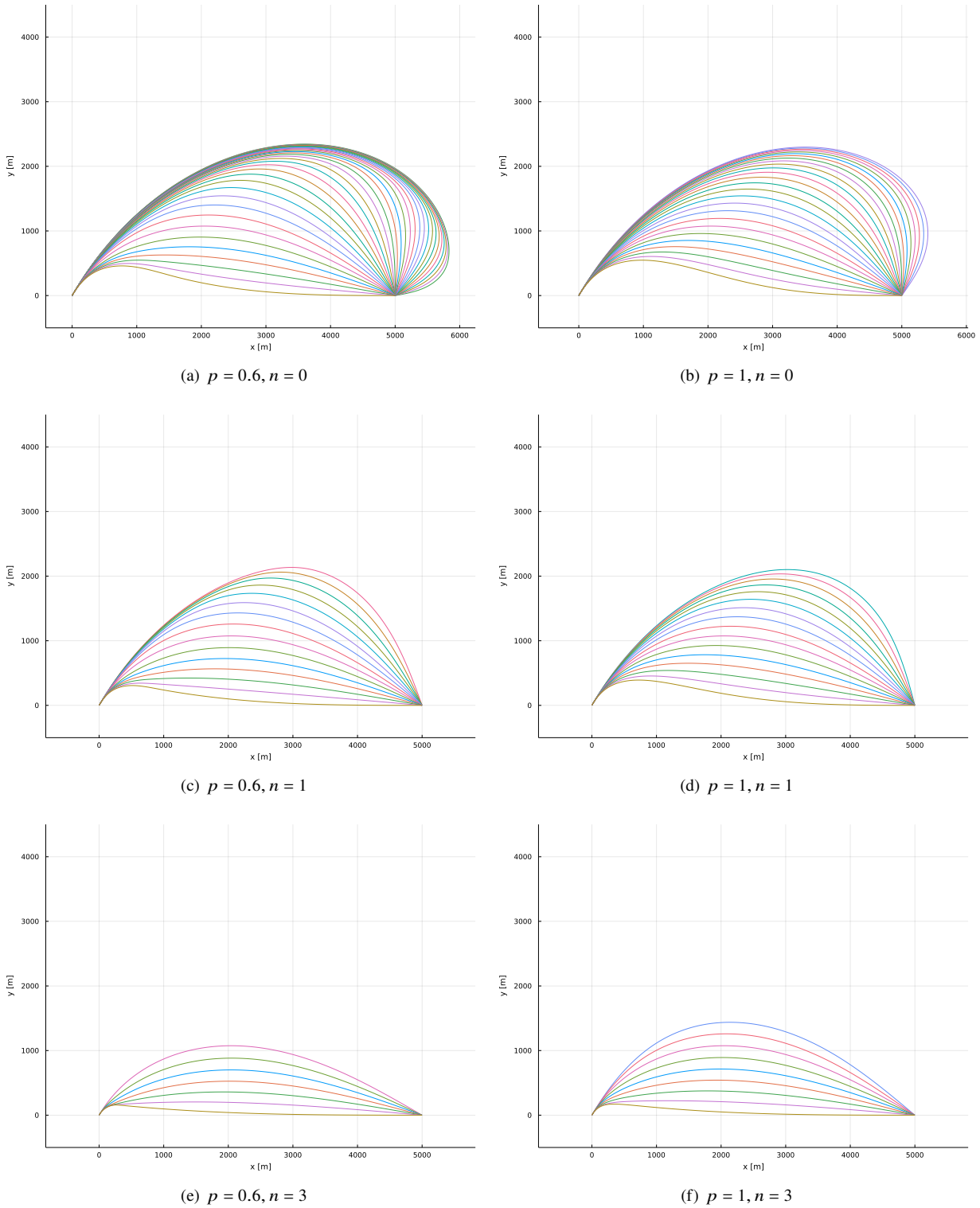
(c) $p = 0.6, n = 1$

(d) $p = 1, n = 1$

(e) $p = 0.6, n = 3$

(f) $p = 1, n = 3$

Fig. 5 Minimum Range and Estimated Feasible Set Boundaries for Each (γ_0, γ_{fd})



(a) $p = 0.6, n = 0$

(b) $p = 1, n = 0$

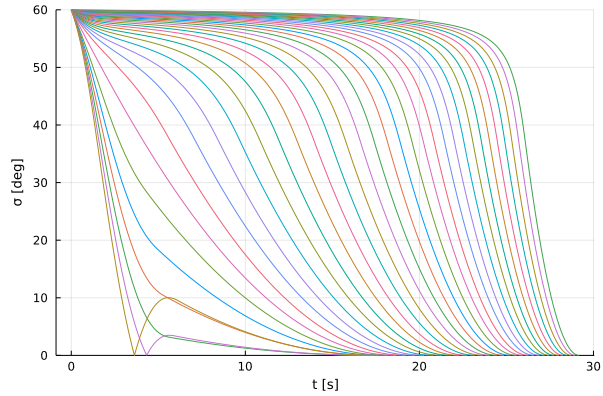
(c) $p = 0.6, n = 1$

(d) $p = 1, n = 1$

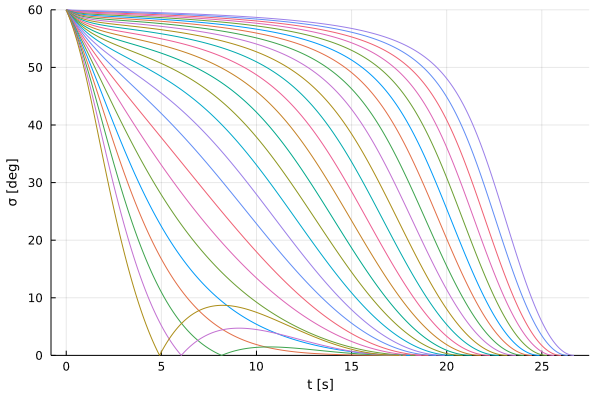
(e) $p = 0.6, n = 3$

(f) $p = 1, n = 3$

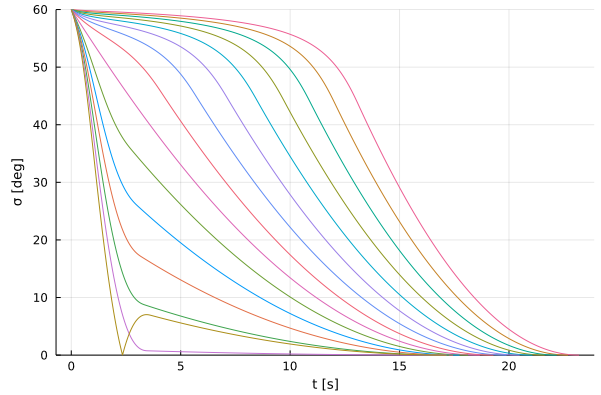
Fig. 6 Two-Dimensional Trajectories for $\gamma_0 = \sigma_{\text{lim}}$



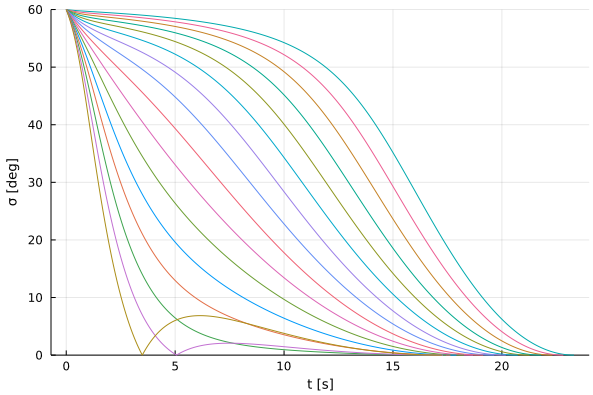
(a) $p = 0.6, n = 0$



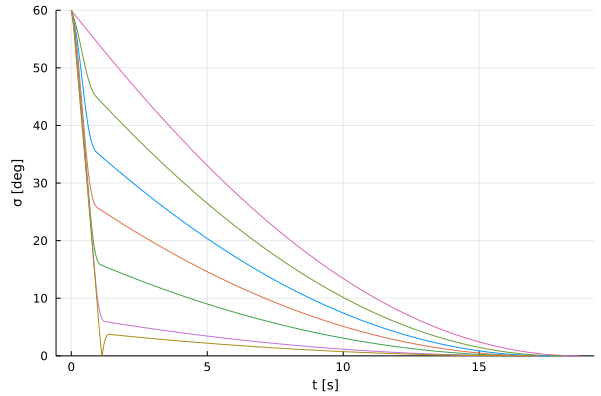
(b) $p = 1, n = 0$



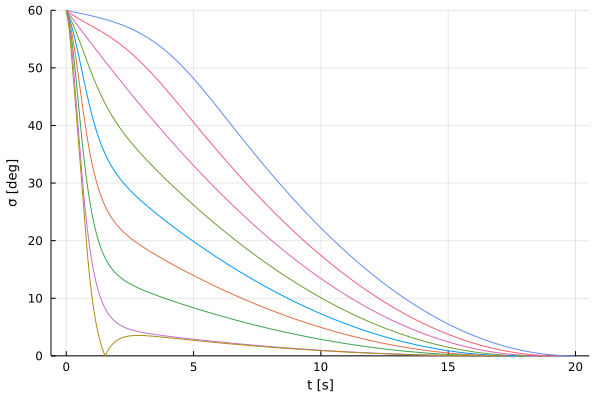
(c) $p = 0.6, n = 1$



(d) $p = 1, n = 1$



(e) $p = 0.6, n = 3$



(f) $p = 1, n = 3$

Fig. 7 Magnitude of Look Angle for $\gamma_0 = \sigma_{\text{lim}}$

(22), the range derivative of $\mathcal{V}$ is given by

$$\mathcal{V}'(r) = e_{\gamma_f} e_{\gamma_f}{}' = \frac{K_r(r) K_\eta(\eta)}{(N-1) r} e_{\gamma_f}{}^2 = \frac{2K_r(r) K_\eta(\eta)}{(N-1) r} \mathcal{V}(r) \tag{B.2}$$

Because of the condition specified by Eq. (20), Eq. (B.2) can be rewritten as

$$\mathcal{V}'(r) \geq \frac{2K_r(r)}{(N-1) r} \mathcal{V}(r) \tag{B.3}$$

The differential inequality above is now given in a separable form. Therefore, applying the comparison lemma [27] to Eq. (B.3) yields,

$$\mathcal{V}(r) \leq \mathcal{V}(r_0) \exp\left[\frac{2}{N-1} \int_{r_0}^{r} \frac{K_r(s)}{s} ds\right] \tag{B.4}$$

Regarding the direction of the inequality sign in Eq. (B.4), one should be aware that $r \leq r_0$ because the range r decreases with respect to time t. Note from the definition in Eq. (B.1) that $\left|e_{\gamma_f}(r)\right| = \sqrt{2\mathcal{V}(r)}$. Thus, Eq. (B.4) can be rewritten about e_{γ_f} as

$$\left|e_{\gamma_f}(r)\right| \leq \left|e_{\gamma_{f_0}}\right| \exp\left[\frac{1}{N-1} \int_{r_0}^{r} \frac{K_r(s)}{s} ds\right] \tag{B.5}$$

where $e_{\gamma_{f_0}} = e_{\gamma_f}(r_0)$. Because $0 \leq r \leq r_0$ and $K_r(r) > 0$ for all $r \in [0, r_0]$, the integral $\int_{r_0}^{r} \frac{K_r(s)}{s} ds$ is negative, and therefore, $\exp\left[\frac{1}{N-1} \int_{r_0}^{r} \frac{K_r(s)}{s} ds\right] \leq 1$.

Equation (B.4) clearly shows that if the condition of Eq. (23) is true, then $V\left(r_f = 0\right) = 0$, because i) the Lyapunov function $\mathcal{V}$ is positive definite by its definition in Eq. (B.1), and ii) the upper bound of $\mathcal{V}$ specified by the right-hand side of Eq. (B.4) at $r = 0$ is equal to zero with Eq. (23) satisfied. The only point in the intersection of $\{\mathcal{V} \geq 0\}$ and $\{\mathcal{V} \leq 0\}$ is $e_{\gamma_f} = 0$.

C. Proof of Corollary 1

(Proof of the first part) Let us first show the necessity part. Without loss of generality, the continuous function $K_r(r)$ can be represented as the sum of the average and deviation as

$$K_r(r) = K_r^* + \tilde{K}_r(r) \tag{C.1}$$

where $\tilde{K}_r(r)$ is an integrable function such that $\int_0^{r_0} \tilde{K}_r(s)\, ds = 0$. Using Eq. (C.1), the following equation can be obtained:

$$\exp\left[\int_{r_0}^{r} \frac{K_r(s)}{s} ds\right] = \left(\frac{r}{r_0}\right)^{K_r^*} \exp\left[\int_{r_0}^{r} \frac{\tilde{K}_r(s)}{s} ds\right] \tag{C.2}$$

Note here that $\exp\left[\int_{r_0}^{r} \frac{\tilde{K}_r(s)}{s} ds\right] > 0, \forall r \in [0, r_0]$. Therefore, if Eq. (23) is true for a $K_r(r)$, then its average over $r \in [0, r_0]$ satisfies $K_r^* > 0$. It is straightforward to show that the logical development in the reverse direction is also valid; hence, the proof for the sufficiency part is obvious.

(Proof of the second part) The proof for the second part follows directly from the first part of this corollary, because $\underline{K}_r > 0 \Rightarrow K_r^* > 0$. Nonetheless, we provide a more detailed explanation here for use in the latter part of this study. If the range-dependent gain is bounded away from zero, it can always be represented as

$$K_r(r) = \underline{K}_r + f_r(r) \tag{C.3}$$

where $\underline{K}_r$ is a positive constant and $f_r(r) \geq 0, \forall r \in [0, r_0]$. Considering the representation given by Eq. (C.3), we have

$$\exp\left[\int_{r_0}^{r} \frac{K_r(s)}{s} ds\right] = \left(\frac{r}{r_0}\right)^{\underline{K}_r} \exp\left[\int_{r_0}^{r} \frac{f_r(s)}{s} ds\right] \tag{C.4}$$

Note here that $0 < \exp\left[\int_{r_0}^{r} \frac{f_r(s)}{s} ds\right] \leq 1, \forall r \in [0, r_0]$ because the upper limit of the integral is less than or equal to the lower limit and the integrand is nonnegative. Equation (C.4) clearly shows that Eq. (23) is true for the range-dependent gain given by Eq. (C.3) with its minimum strictly greater than zero.

D. Proof of Corollary 2

Using the relations Eqs. (19) and (B.5) in Eq. (18), the magnitude of the bias command can be written as

$$\left|u_{\text{aug}}(r)\right| \leq \left|e_{\gamma_{f_0}}\right| K_\eta(\eta) \frac{K_r(r)}{r} \exp\left[\frac{1}{N-1} \int_{r_0}^{r} \frac{K_r(s)}{s} ds\right] \tag{D.1}$$

The additional correction input u_{aug} does not blow up during the engagement if the term $\frac{K_r(r)}{r} \exp\left[\frac{1}{N-1} \int_{r_0}^{r} \frac{K_r(s)}{s} ds\right]$ is bounded. Moreover, it is obvious from Eq. (D.1) that the strengthened condition given by Eq. (25) results in zero bias command at the end of engagement.

Using Eqs. (C.1) and (C.2), the term on the right-hand side of Eq. (D.1) pertaining to $K_r(r)$ can be rewritten as

$$\frac{K_r(r)}{r} \exp\left[\frac{1}{N-1} \int_{r_0}^{r} \frac{K_r(s)}{s} ds\right] = \frac{K_r^* + \tilde{K}_r(r)}{r} \left(\frac{r}{r_0}\right)^{\frac{K_r^*}{N-1}} \exp\left[\frac{1}{N-1} \int_{r_0}^{r} \frac{\tilde{K}_r(s)}{s} ds\right] \tag{D.2}$$

Equation (D.2) indicates that the term of interest is proportional to $r^{\frac{K_r^*}{N-1}-1}$. Therefore, one can easily show that Eq. (25) is satisfied if and only if Eq. (26) is true. Additionally, as a direct consequence, Eq. (25) is satisfied for $K_r(r)$ given by Eq. (C.3) if Eq. (27) holds because $\underline{K}_r > N-1 \Rightarrow K_r^* > N-1$.

E. Proof of Theorem 2

The proof centers around the study of Eq. (21) as it describes the evolution of η over r under the proposed guidance law. Because $0 < \sqrt{1-\eta^2} \leq 1$ for $\forall \eta \in (-1, 1)$, the upper bound for $K_\eta(\eta)$ in Eq. (31) can be written again as

$$K_\eta(\eta) \leq \overline{K}_\eta \leq \frac{\overline{K}_\eta}{\sqrt{1-\eta^2}} \tag{E.1}$$

for any $\overline{K}_\eta \geq 1$. Using Eqs. (B.5) and (E.1), the absolute value of the term inside the bracket in Eq. (21) is shown to be bounded by the following:

$$\frac{\sqrt{1-\eta^2}}{(N-1)|\eta|} K_r(r) K_\eta(\eta) \left|e_{\gamma_f}\right| \leq \frac{g(r)}{|\eta|} \tag{E.2}$$

with

$$g(r) \triangleq \frac{\overline{K}_\eta \left|e_{\gamma_{f_0}}\right|}{N-1} K_r(r) \exp\left[\frac{1}{N-1}\int_{r_0}^{r} \frac{K_r(s)}{s} ds\right] \geq 0 \tag{E.3}$$

Consequentially, the following inequality is true.

$$1 - \frac{g(r)}{|\eta|} \leq 1 - \frac{\sqrt{1-\eta^2}}{(N-1)\eta} K_r(r) K_\eta(\eta) e_{\gamma_f} \leq 1 + \frac{g(r)}{|\eta|} \tag{E.4}$$

Now, consider the following scalar function to analyze the properties of $\eta(r)$.

$$\mathcal{V}_\eta(r) = \frac{1}{2}\eta^2 \tag{E.5}$$

Note that $\mathcal{V}_\eta \geq 0$ and $\mathcal{V}_\eta = 0$ if and only if $\eta = 0$. Additionally, note that $|\eta| = \sqrt{2\mathcal{V}_\eta}$ and $\mathcal{V}_\eta{}' = \eta\eta'$. Considering Eqs. (21) and (E.4), the derivative of $\mathcal{V}_\eta$ with respect to r satisfies

$$\mathcal{V}_\eta{}' = 2(N-1)\frac{\mathcal{V}_\eta}{r}\left[1 - \frac{\sqrt{1-\eta^2}}{(N-1)\eta} K_r(r) K_\eta(\eta) e_{\gamma_f}\right] \geq 2(N-1)\frac{\mathcal{V}_\eta}{r}\left[1 - \frac{g(r)}{\sqrt{2\mathcal{V}_\eta}}\right] \tag{E.6}$$

Let $U(r)$ be the solution of

$$U'(r) = 2(N-1)\frac{U(r)}{r}\left[1 - \frac{g(r)}{\sqrt{2U(r)}}\right], \quad U(r_0) = V_\eta(r_0) \tag{E.7}$$

Equation (E.7) is a Bernoulli differential equation. The closed-form solution for Eq. (E.7) can be obtained as [26]

$$U(r) = \left[r^{N-1}\left\{\frac{\sqrt{V_\eta(r_0)}}{{r_0}^{N-1}} - \frac{N-1}{\sqrt{2}}\int_{r_0}^{r} \frac{g(s)}{s^N} ds\right\}\right]^2 \tag{E.8}$$

Applying the comparison lemma [27] to Eq. (E.6), yields

$$\mathcal{V}_\eta(r) \le U(r), \quad \forall r \in [0, r_0] \tag{E.9}$$

Equation (E.9) can be rewritten about η as

$$|\eta(r)| \le r^{N-1}\left\{\frac{|\eta_0|}{{r_0}^{N-1}} - (N-1)\int_{r_0}^{r}\frac{g(s)}{s^N}ds\right\} \tag{E.10}$$

where $\eta_0 = \eta(r_0)$. The right-hand side of Eq. (E.10) becomes zero at $r = 0$ because $N > 1$ and $\int_{r_0}^{r}\frac{g(s)}{s^N}ds \le 0$. In conjunction with the property that an absolute value is always nonnegative, this clearly proves $\eta\left(r_f = 0\right) = 0$.

F. Proof of Theorem 3

If the condition in Eq. (32) is satisfied, it follows from Eq. (B.5) that

$$K_r(r)\left|e_{\gamma_f}(r)\right| \le \frac{(N-1)\eta_{\lim}}{K_{\eta_{\lim}}\sqrt{1-\eta_{\lim}^2}}, \ \forall r \in [0, r_0] \tag{F.1}$$

Note that the relation $\tan\sigma_{\lim} = \frac{\eta_{\lim}}{\sqrt{1-{\eta_{\lim}}^2}}$ is used in the derivation of Eq. (F.1).

Evaluating $\eta\eta'$ at $\eta = \pm\eta_{\lim}$ by using Eq. (21) yields

$$[\eta\eta']|_{\eta=\pm\eta_{\lim}} = (N-1)\frac{{\eta_{\lim}}^2}{r}\left[1 \mp \frac{K_{\eta_{\lim}}\sqrt{1-\eta_{\lim}^2}}{(N-1)\eta_{\lim}}K_r(r)\, e_{\gamma_f}\right] \tag{F.2}$$

Considering the inequality of Eq. (F.1), the term in the bracket of Eq. (F.2) is always greater than or equal to zero, which guarantees $[\eta\eta']|_{\eta=\pm\eta_{\lim}} \ge 0$ as a consequence. The condition given by Eq. (17) holds, and therefore, the look angle neither grows larger than $\sigma_{\lim}$ nor diminishes smaller than $-\sigma_{\lim}$ in light of the discussion in Sec. II.C.

G. Proof of Corollary 3

Rewriting Eq. (36) gives

$$\overline{K}_r \le \frac{(N-1)\tan\sigma_{\lim}}{\left|e_{\gamma_{f_0}}\right| K_{\eta_{\lim}}} \tag{G.1}$$

It is obvious from $0 \le r < r_0$, $N > 1$, and $K_r(r) > 0$ that

$$K_r(r)\exp\left[\frac{1}{N-1}\int_{r_0}^{r}\frac{K_r(s)}{s}ds\right] \le K_r(r) \le \overline{K}_r \tag{G.2}$$

From Eqs. (G.1) and (G.2), one can conclude that Eq. (36) is a sufficient condition for Eq. (32) in Theorem 3 to hold.

Additionally, Eqs. (7) and (8) indicate that $e_{\gamma_{f_0}} = -\frac{\gamma_0}{N-1} - \gamma_{f_d}$ when $\gamma_0 = \sigma_0$. Equations (37) and (38) are simply obtained by considering the relation for the ground-to-ground attack case and rearranging Eq. (36) with respect to γ_0 and γ_{f_d}, respectively.

H. Proof of Theorem 4

If $e_{\gamma_{f_0}} = 0$, the error e_{γ_f} will be identically zero throughout the entire interval, and the analysis for this case is meaningless. Thus, the proof here considers the case in which $e_{\gamma_{f_0}} \neq 0$.

Consider the Lyapunov candidate function $\mathcal{V}(r)$ defined by Eq. (B.1) for the analysis of convergence behavior. With u_{aug} given by Eq. (42), the derivative of $\mathcal{V}$ with respect to r can be obtained by using Eq. (44) as follows:

$$\mathcal{V}'(r) = \frac{K_r(r) K_\eta(\eta)}{(N-1) r} \left|e_{\gamma_f}\right|^{1+p} = \frac{K_r(r) K_\eta(\eta)}{(N-1) r} \{2\mathcal{V}(r)\}^{\frac{1+p}{2}} \tag{H.1}$$

If K_η satisfies Eq. (20), then Eq. (H.1) can be rewritten as

$$\{\mathcal{V}(r)\}^{-\frac{1+p}{2}} \mathcal{V}'(r) \geq \frac{2^{\frac{1+p}{2}} K_r(r)}{(N-1) r} \tag{H.2}$$

The differential inequality in Eq. (H.2) can be solved by integration as

$$\{2\mathcal{V}(r)\}^{\frac{1-p}{2}} \leq \alpha(r) \tag{H.3}$$

where

$$\alpha(r) \triangleq \{2\mathcal{V}(r_0)\}^{\frac{1-p}{2}} + \frac{1-p}{N-1} \int_{r_0}^{r} \frac{K_r(s)}{s} ds \tag{H.4}$$

Because $N > 1$, $p < 1$, $K_r(r) > 0$, and $r \leq r_0$, the function $\alpha(r)$ is continuous and monotonically increasing in r. Additionally, it is obvious from Eq. (H.4) that $\alpha(r_0) > 0$ since $e_{\gamma_{f_0}} \neq 0$.

If $K_r(r)$ satisfies Eq. (45), we have $\lim_{r \to 0} \alpha(r) < 0$. Therefore, according to Bolzano's theorem [28], there exists $r^* \in (0, r_0)$ such that $\alpha(r^*) = 0$. This automatically implies the existence of $r^* \in (0, r_0)$ such that $\mathcal{V}(r^*) = 0$ because $\mathcal{V}(r)$ is always nonnegative by definition. Therefore, e_{γ_f} converges to zero before interception.

In summary, the behavior of e_{γ_f} can be described as follows:

$$\begin{aligned} \left|e_{\gamma_f}(r)\right|^{1-p} &\leq \left|e_{\gamma_{f_0}}\right|^{1-p} + \frac{1-p}{N-1} \int_{r_0}^{r} \frac{K_r(s)}{s} ds, \quad && \forall r \in [r^*, r_0] \\ e_{\gamma_f}(r) &= 0, && \forall r \in [0, r^*] \end{aligned} \tag{H.5}$$

for some $r^* \in (0, r_0)$ such that $\alpha(r^*) = 0$.

I. Proof of Theorem 5

Considering the behavior of e_{γ_f} described in Eq. (H.5), the following inequality is true if Eq. (46) is satisfied.

$$K_r(r)\left|e_{\gamma_f}(r)\right|^p \leq \frac{(N-1)\,\eta_{\lim}}{K_{\eta_{\lim}}\sqrt{1-\eta_{\lim}^2}}, \quad \forall r \in [0, r_0] \tag{I.1}$$

Note that $\int_{r_0}^{r} \frac{K_r(s)}{s} ds \leq 0$ for $r \leq r_0$, and the rest of the proof follows the same logical flow shown previously in Theorem 3.

J. Proof of Corollary 4

It is clear that $K_r(r) \leq \overline{K}_r$ and

$$\left[\left|e_{\gamma_{f_0}}\right|^{1-p} + \frac{1-p}{N-1}\int_{r_0}^{r} \frac{K_r(s)}{s} ds\right]^{\frac{p}{1-p}} \leq \left|e_{\gamma_{f_0}}\right|^p \tag{J.1}$$

Therefore, the condition given by Eq. (I.1) is satisfied if

$$\overline{K}_r \left|e_{\gamma_{f_0}}\right|^p \leq \frac{(N-1)\tan\sigma_{\lim}}{K_{\eta_{\lim}}} \tag{J.2}$$

Rewriting the above sufficient condition about $e_{\gamma_{f_0}}$ gives an estimate for the range of permissible initial conditions as in Eq. (47).

References

[1] Manchester, I. R., and Savkin, A. V., "Circular-Navigation-Guidance Law for Precision Missile/Target Engagements," *Journal of Guidance, Control, and Dynamics*, Vol. 29, No. 2, 2006, pp. 314–320. doi:10.2514/1.13275.

[2] Park, B.-G., Jeon, B. J., Kim, T.-H., Tahk, M.-J., and Kim, Y.-H., "Composite Guidance Law for Impact Angle Control of Tactical Missiles with Passive Seekers," *Asia-Pacific International Symposium on Aerospace Technology*, Seoul, Korea, 2012.

[3] Kim, T.-H., Park, B.-G., and Tahk, M.-J., "Bias-Shaping Method for Biased Proportional Navigation with Terminal-Angle Constraint," *Journal of Guidance, Control, and Dynamics*, Vol. 36, No. 6, 2013, pp. 1810–1816. doi:10.2514/1.59252.

[4] Park, B.-G., "Impact Angle Control Guidance Law Considering the Seekers Field-of-View Limits," Ph.D. thesis, Korea Advanced Institute of Science and Technology, Daejeon, Republic of Korea, 2013.

[5] Park, B.-G., Kim, T.-H., and Tahk, M.-J., "Optimal Impact Angle Control Guidance Law Considering the Seeker's Field-of-View Limits," *Proceedings of the Institution of Mechanical Engineers, Part G: Journal of Aerospace Engineering*, Vol. 227, No. 8, 2013, pp. 1347–1364. doi:10.1177/0954410012452367.

[6] Erer, K. S., Tekin, R., and Ozgoren, M. K., "Look Angle Constrained Impact Angle Control Based on Proportional Navigation," *AIAA Guidance, Navigation, and Control Conference*, Kissimmee, FL, 2015. doi:10.2514/6.2015-0091.

[7] Tekin, R., and Erer, K. S., "Switched-Gain Guidance for Impact Angle Control under Physical Constraints," *Journal of Guidance, Control, and Dynamics*, Vol. 38, No. 2, 2015, pp. 205–216. doi:10.2514/1.G000766.

[8] He, S., and Lin, D., "A Robust Impact Angle Constraint Guidance Law with Seeker's Field-of-View Limit," *Transactions of the Institute of Measurement and Control*, Vol. 37, No. 3, 2015, pp. 317–328. doi:10.1177/0142331214538278.

[9] Ratnoo, A., "Analysis of Two-Stage Proportional Navigation with Heading Constraints," *Journal of Guidance, Control, and Dynamics*, Vol. 39, No. 1, 2016, pp. 197–200. doi:10.2514/1.G001533.

[10] Park, B.-G., Kim, T.-H., and Tahk, M.-J., "Range-to-Go Weighted Optimal Guidance with Impact Angle Constraint and Seeker's Look Angle Limits," *IEEE Transactions on Aerospace and Electronic Systems*, Vol. 52, No. 3, 2016, pp. 1241–1256. doi:10.1109/TAES.2016.150415.

[11] Liu, X., Shen, Z., and Lu, P., "Closed-Loop Optimization of Guidance Gain for Constrained Impact," *Journal of Guidance, Control, and Dynamics*, Vol. 40, No. 2, 2017, pp. 453–460. doi:10.2514/1.G000323.

[12] Ratnoo, A., "Nonswitching Guidance Law for Trajectory Shaping Control," *Journal of Guidance, Control, and Dynamics*, Vol. 40, No. 10, 2017, pp. 2721–2728. doi:10.2514/1.G002459.

[13] Ghosh, S., Yakimenko, O. A., Davis, D. T., and Chung, T. H., "Unmanned Aerial Vehicle Guidance for an All-Aspect Approach to a Stationary Point," *Journal of Guidance, Control, and Dynamics*, Vol. 40, No. 11, 2017, pp. 2871–2888. doi:10.2514/1.G002614.

[14] Kim, H.-G., Lee, J.-Y., and Kim, H. J., "Look Angle Constrained Impact Angle Control Guidance Law for Homing Missiles With Bearings-Only Measurements," *IEEE Transactions on Aerospace and Electronic Systems*, Vol. 54, No. 6, 2018, pp. 3096–3107. doi:10.1109/TAES.2018.2843600.

[15] Kim, J., Cho, N., and Kim, Y., "Field-of-View Constrained Impact Angle Control Guidance Guaranteeing Error Convergence Before Interception," *AIAA Guidance, Navigation, and Control Conference*, San Diego, CA, 2019. doi:10.2514/6.2019-1927.

[16] Kim, J., Cho, N., and Kim, Y., "Field-of-View-Constrained Impact Angle Control Guidance with Error Convergence before Interception Considering Speed Changes," *Proceedings of the Institution of Mechanical Engineers, Part G: Journal of Aerospace Engineering*, Vol. 235, No. 2, 2021, pp. 238–256. doi:10.1177/0954410020942010.

[17] Liu, B., Hou, M., and Li, Y., "Field-of-View and Impact Angle Constrained Guidance Law for Missiles With Time-Varying Velocities," *IEEE Access*, Vol. 7, 2019, pp. 61717–61727. doi:10.1109/ACCESS.2019.2916798.

[18] Liu, B., Hou, M., and Feng, D., "Nonlinear Mapping Based Impact Angle Control Guidance with Seeker's Field-of-View Constraint," *Aerospace Science and Technology*, Vol. 86, 2019, pp. 724–736. doi:10.1016/j.ast.2019.02.009.

[19] Sharma, Y. R., and Ratnoo, A., "A Bearings-Only Trajectory Shaping Guidance Law With Look-Angle Constraint," *IEEE Transactions on Aerospace and Electronic Systems*, Vol. 55, No. 6, 2019, pp. 3303–3315. doi:10.1109/TAES.2019.2906090.

[20] Zhou, S., Zhang, S., and Wang, D., "Impact Angle Control Guidance Law With Seeker's Field-of-View Constraint Based on Logarithm Barrier Lyapunov Function," *IEEE Access*, Vol. 8, 2020, pp. 68268–68279. doi:10.1109/ACCESS.2020.2986355.

[21] Park, B.-G., Kwon, H.-H., Kim, Y.-H., and Kim, T.-H., "Composite Guidance Scheme for Impact Angle Control Against a Nonmaneuvering Moving Target," *Journal of Guidance, Control, and Dynamics*, Vol. 39, No. 5, 2016, pp. 1132–1139. doi:10.2514/1.G001547.

[22] Park, B.-G., Kim, T.-H., and Tahk, M.-J., "Biased PNG With Terminal-Angle Constraint for Intercepting Nonmaneuvering Targets Under Physical Constraints," *IEEE Transactions on Aerospace and Electronic Systems*, Vol. 53, No. 3, 2017, pp. 1562–1572. doi:10.1109/TAES.2017.2667518.

[23] Lee, S., Ann, S., Cho, N., and Kim, Y., "Capturability of Guidance Laws for Interception of Nonmaneuvering Target with Field-of-View Limit," *Journal of Guidance, Control, and Dynamics*, Vol. 42, No. 4, 2019, pp. 869–884. doi:10.2514/1.G003860.

[24] Lee, S., and Kim, Y., "Capturability of Impact-Angle Control Composite Guidance Law Considering Field-of-View Limit," *IEEE Transactions on Aerospace and Electronic Systems*, Vol. 56, No. 2, 2020, pp. 1077–1093. doi:10.1109/TAES.2019.2925485.

[25] Cho, N., Kim, J., and Lee, S., "Feasible Initial Conditions for Bias Proportional Navigation Guidance Laws Under Look Angle Constraints," *28th Mediterranean Conference on Control and Automation*, Virtual (Saint-Raphael, France), 2020. doi:10.1109/MED48518.2020.9183280.

[26] Zwillinger, D., *Handbook of Differential Equations*, 3rd ed., Academic Press, Boston, MA, 1997, pp. 214–216.

[27] Khalil, H. K., *Nonlinear Systems*, 3rd ed., Prentice Hall, Upper Saddle River, NJ, USA, 2002, pp. 102–104.

[28] Russ, S. B., "A Translation of Bolzano's Paper on the Intermediate Value Theorem," *Historia Mathematica*, Vol. 7, No. 2, 1980, pp. 156–185. doi:10.1016/0315-0860(80)90036-1.



https://dspace.org/

Generalized analysis of biased proportional navigation guidance with fractional power error feedback

Cho, Namhoon; Kim, Jinrae; Lee, Seokwon; Kim, Youdan

2022-06-03
AIAA
https://doi.org/10.2514/1.G006850
Cho N, Kim J, Lee S, Kim Y. (2022) Generalized analysis of biased proportional navigation guidance with fractional power error feedback, Journal of Guidance, Control, and Dynamics, Volume 45, Number 9, September 2022, pp. 1598-1613

Downloaded from a DSpace repository. https://dspace.org/